DISCLAIMER

This report was prepared as an account of work sponsored by an agency of the United States Government. Neither the United States Government nor any agency thereof, nor any of their employees, makes any warranty, express or implied, or assumes any legal liability or responsibility for the accuracy, completeness, or usefulness of any information, apparatus, product, or process disclosed, or represents that its use would not infringe privately owned rights. Reference herein to any specific commercial product, process, or service by trade name, trademark, manufacturer, or otherwise does not necessarily constitute or imply its endorsement, recommendation, or favoring by the United States Government or any agency thereof. The views and opinions of authors expressed herein do not necessarily state or reflect those of the United States Government or any agency thereof. Reference herein to any social initiative (including but not limited to Diversity, Equity, and Inclusion (DEI); Community Benefits Plans (CBP); Justice 40; etc.) is made by the Author independent of any current requirement by the United States Government and does not constitute or imply endorsement, recommendation, or support by the United States Government or any agency thereof.

LBNL-2001667

University of Hawai‘i

Shallow Geothermal Resources

Energy Technology Innovation Partnership Project Final Report

January 2025

Christine Doughty, Jianjun Hu, Craig Ulrich, Sean Murphy, Pat Dobson
Lawrence Berkeley National Laboratory

Nicole Lautze, Donald Thomas
University of Hawai‘i (UH) at Manoa

Mike Campton
National Renewable Energy Laboratory

List of Acronyms

GHE	geothermal heat exchanger
NPV	net present value
TOUGH	Transport of Unsaturated Groundwater and Heat
UH	University of Hawai‘i

Executive Summary

Scientists at Lawrence Berkeley National Laboratory (Berkeley Lab) have teamed up with the University of Hawai‘i at Manoa (UH Manoa) through the U.S. Department of Energy’s Energy Technology Innovation Partnership Project to evaluate the technological and market feasibility of shallow geothermal heat exchanger (GHE) technology. UH requested this analysis to evaluate opportunities in building cooling, energy efficiency, and emissions reduction applications in Hawai‘i. UH has an abundance of geologic and geothermal data and is looking to the national labs’ expertise to execute this analysis. UH is also interested in investigating policy, regulatory, and business conditions advantageous for implementation of a pilot project and more broad deployment of this technology in Hawai‘i.

In many locations around the world, the demands for heating and cooling are roughly balanced over the course of the year, so GHEs do not cause significant long-term changes in subsurface temperature. This is not the case in Hawai’i, where the demand for heating is very small, meaning that, over time, GHEs will add heat to the subsurface. If temperatures increase significantly, GHE systems will not work as designed. Regional groundwater flow has the potential to sweep heated water away from boreholes, thereby maintaining the functionality of the GHE system. Significant regional groundwater flow requires two things: a sufficiently large driving hydraulic head gradient (usually closely related to surface topography), and sufficient porosity and permeability to enable groundwater to flow in large enough quantities to enable near-borehole temperatures to be maintained at ambient values. Hawai‘i’s volcanic terrain offers ample surface topographic variation. The lava itself shows an extremely large range of porosity and permeability, so sites with large enough values of these properties must be selected. Numerical modeling of coupled groundwater and heat flow can be used to determine how large is large enough. Primarily, closed-loop systems have been investigated. Other options considered are open-loop systems and using cool seawater as the chilling source.

Project work investigated the feasibility of GHE technology at two scales. At the island scale, GIS layers of various attributes relevant for GHE were combined to develop an overall favorability map for employing GHE in Hawai‘i. At the local scale, a hydrogeologic model for the subsurface component of a closed-loop system was developed for the Stan Sheriff Center at the UH Manoa campus. This site is considered promising because the rock below and immediately downgradient of the borefield is highly permeable, consisting of a subsurface karst system (limestone containing high-permeability open channels), which is underlain by a thick, high-permeability fractured basalt. Moreover, the site is near the base of the Ko‘olau Range, providing a large hydraulic head gradient. Thus, groundwater flow through the site is expected to be large, enabling efficient removal of heated groundwater. A full-GHE-system model of the site was also developed, with a simplified representation of the subsurface, in which groundwater flow is not considered and heat transfer is purely by conduction. Using the building cooling load data provided by UH, simulation results show that with groundwater flow present, a GHE can operate successfully for at least 10 years, but with no groundwater flow, the subsurface begins to heat up after only one year of operation, making the GHE unviable within 2-6 years. The team also developed a techno-economic model for this site to compare the cost of cooling using a GHE system with the costs of operating the current air-conditioning system. The GHE system is advantageous economically if favorable tax incentives and interest rates can be obtained.

Table of Contents

List of Figures

List of Tables

1. Introduction

This study is a U.S. Department of Energy's Energy Technology Innovation Partnership Project, which seeks to partner U.S. Department of Energy national laboratory scientists with remote, coastal, and island communities looking to transform their energy systems and increase energy resilience. The University of Hawai‘i (UH) identified goals for this project, including analyzing the potential for geothermal cooling in buildings across its 10 campuses by modeling shallow geologic conditions and building heating and cooling loads and evaluating potential geothermal technologies that could improve energy efficiency and significantly increase energy reliability for these communities. (e.g., Liu et al. 2023).

This project builds upon an earlier assessment by Dores and Lautze (2020), who evaluated a variety of scenarios relating to the applicability of ground-source heat exchangers for space cooling in Hawai‘i. They examined a number of important parameters for six of the Hawaiian Islands, such as shallow geology, depth to water table, and groundwater and measured air temperatures. These datasets were then projected onto GIS maps of each of the studied islands. For effective cooling to occur using geothermal heat exchanger (GHE) technology, a threshold maximum water table depth of 80 m was assigned. The groundwater temperature was used as a proxy for subsurface ground temperature at the same depth as the groundwater measurement, and a comparison was made between air and subsurface temperatures throughout the year for the major population areas on the four most populated islands. Using literature values for the thermal conductivities of the four main rock types—alluvium and fill, basalts and other volcanic rocks, sand and dune deposits, and limestone and reef deposits—the basalts and limestones were identified as having the most prospective thermal properties for deploying GHE systems. Both seasonal and yearly operational scenarios were evaluated. The study concluded that space cooling would be feasible using GHE systems in Hawai‘i, and that more detailed modeling would be needed to assess the impacts of groundwater flow, which enables heat to be swept away by a process known as convective heat transfer.

The current project has two primary objectives: (1) expanding the GIS-based screening methodology of Dores and Lautze (2020) to further assess the feasibility of deploying GHE technology in Hawai‘i; and (2) conducting a more detailed technical and economic assessment of the potential for developing such a system for cooling of the Stan Sheriff Center athletic complex at the UH Manoa campus. This involves developing a detailed 3D geologic model of the area that can be used to create a hydrogeologic framework for numerical modeling. One of the key concerns for applying GHE in tropical environments is that heat is continually added to the subsurface with only cooling being used, and that lateral flow of groundwater is required to sweep the heat away so that the system can continue to operate.

Early results of this work were presented at the 2024 Geothermal Rising conference (Doughty et al. 2024).

2. GIS-Based Screening Criteria for GHE in Hawai‘i

As noted, Dores and Lautze (2020) used the shallow geology, depth to water table, and groundwater and air temperatures to help identify prospective areas within six of the Hawaiian Islands where GHE might be feasible. Our team expanded this list of parameters to include additional screening criteria that would be useful in evaluating the suitability of a particular location for installing a closed-loop GHE system on O‘ahu. We also looked at the potential of using open-loop systems as well as seawater cooling systems (e.g., Leraand and Van Ryzin 1995), but this evaluation is confined to closed-loop GHE applications. The criteria consist of a variety of physical (i.e., geographic, geologic, hydrologic), ecological/environmental, and cultural factors that would influence the viability of deploying a GHE system. Two examples of these GIS screening criteria (soil permeability and the locations of schools and U.S. Department of Defense land) on O‘ahu are displayed in Figure 1. Table 1 summarizes these features and provides some suggestions as to what might constitute favorable versus unfavorable conditions for each of these parameters. Many of these parameters can be mapped using corresponding GIS layers, so that multiple factors can be examined and areas that have favorable or unfavorable conditions can be easily identified using this approach.

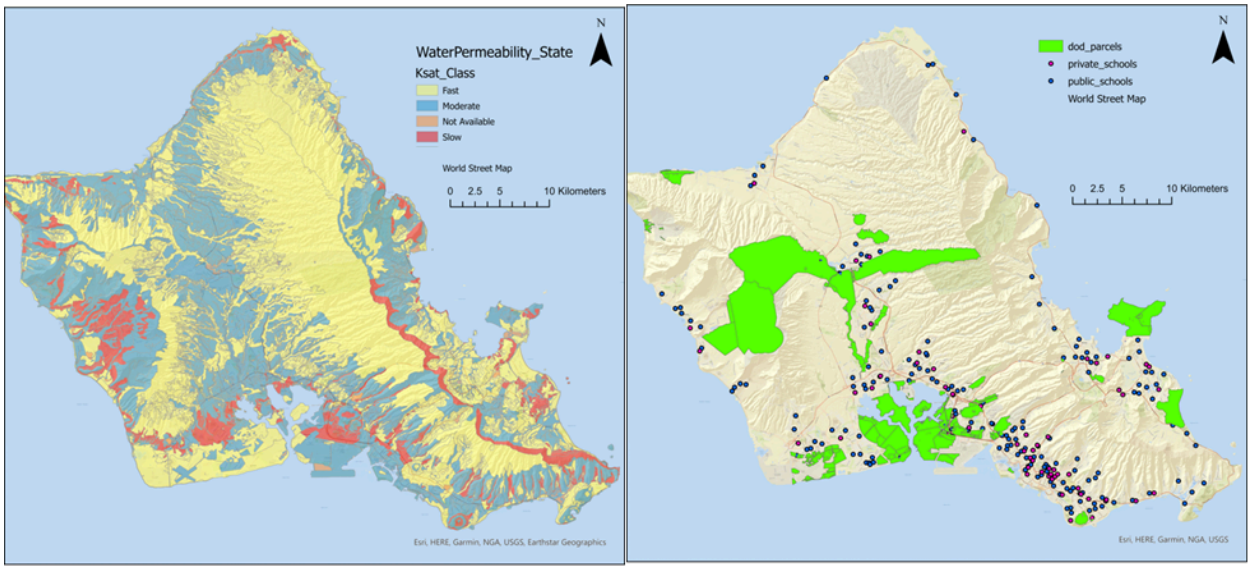

Figure 1. Left: GIS map of O‘ahu depicting different soil permeability zones; Ksat Class refers to how fast material drains. Right: Locations of U.S. Department of Defense lands and public and private schools on O‘ahu. See Table 1 for data sources.

2.1 Key Physical Parameters

A number of physical parameters are important for GHE installations. To meet the needs of cooling, the groundwater temperature needs to be low enough to be able to effectively cool buildings. Given that the GHE system will not be balanced between heating and cooling, there needs to be sufficient groundwater flow so that heat can be swept away from the boreholes. Having a sufficiently sloped piezometric surface and hydraulic head will promote higher lateral water flow rates needed to remove the heat, but it is also important to consider the ground surface slope (i.e., from the digital elevation model), as it will add complexity to siting the GHE. The subsurface geology needs to have high enough permeability to facilitate a high flux of groundwater flow through the area where the borefield will be situated. Finally, the boreholes need to be located in an area with a fairly shallow water table, as the bulk of the borehole length needs to be located in water-saturated rock below

the water table, as opposed to the partially-saturated rock above the water table, known as the vadose zone, where pore spaces contain both water and air. This location promotes effective heat transfer between the closed-loop boreholes and the surroundings, considering both thermal conduction, since saturated rock has much higher thermal conductivity than partially-saturated rock, and convection by groundwater moving past the borehole, which only occurs in the water-saturated zone.

2.2 Key Ecological and Environmental Parameters

The siting of a GHE will require drilling numerous boreholes. This may not be possible in densely vegetated and forested lands and in areas that have endangered species. There are areas with restricted watersheds that might not permit GHE deployment. There may be conflicts with the existing use of the subsurface for freshwater production or water injection. The use of a closed-loop system may minimize such conflicts. Areas with existing wells will be better characterized with respect to their hydrogeology, which can help develop better constrained models that can be used to predict long-term GHE performance and estimate the cost-effectiveness of such systems.

2.3 Key Cultural Parameters

There are a variety of cultural factors that may promote or restrict the deployment of GHE systems. Areas with an elevated community heat index and high cooling needs may be good candidates for such a system. Older homes often lack efficient cooling systems, so developing GHE systems within those neighborhoods could have beneficial impacts. Some organizations, such as schools and the U.S. military, have prioritized making their sites more resilient, so they may be good candidates for GHE cooling systems. There are some locations, such as national parks and sites of cultural and archeological sensitivity, where such systems cannot be deployed.

Table 1. Summary of Key Screening Parameters for Siting Closed-Loop GHE Installations

Parameter	Importance	Data Range	Favorable	Acceptable	Unfavorable	Comments	GIS Data Source
Physical Parameters							
Elevation	Useful	0 to >3,000 m	0–20 m	20–100 m	>100 m	Proxy for depth to water table	https://planning.hawaii.gov/gis/download-gis-data-expanded/
Slope	Useful	0 to 90°	2–5°	0–2°, 5–10°	>10°	Higher slope harder to build on, but provides steeper hydrologic gradient.	Calculated from elevation model
Depth to Water Table	Critical	0 to >100 m	0–10 m	10–80 m	>80 m	GHE needs to be deployed within saturated zone for heat to be dissipated effectively via convection.	Dores and Lautze, 2020 https://waterdata.usgs.gov/hi/nwis/gw/
Geology	Critical	Basalt lava flows, breccia, tuff, limestone, alluvium	Fractured basalt, limestone		Unfractured basalt (dike-rich zones)	Fractured basalts typically have good horizontal permeability. Caverns in limestone may be problematic for drilling and well completion.	https://ngmdb.usgs.gov/Prodesc/proddesc_111883.htm
Soil Moisture	Useful	Arid to very wet (7 classes)	Wet zones	Intermediate zones	Arid zones	Wet zones likely have higher subsurface flow; arid zones may have deeper water table.	https://www.sciencebase.gov/catalog/item/57a902e8e4b05e859bdf3c83
Permeability	Critical	Ksat classes (very fast, fast, moderate, slow)	High or very high permeability	Intermediate permeability	Low permeability	High permeability zones more likely to effectively dissipate heat.	http://gis.ctahr.hawaii.edu/SoilAtlas

Groundwater Temperature	Critical		<20°C	20–25°C	>25°C	Warm water less favorable for cooling applications.	https://www.higp.hawaii.edu/hggrc/projects/hi-play-fairway/pf-project-data/
Tsunami Zone	Useful		Outside		Inside	Borehole installations are below ground surface, so this should be less critical.	https://www.honolulugis.org/apps/39a9e07068a14d01a85b437adcf50beb/explore
Ecological and Environmental Parameters							
Vegetation Cover	Useful	Bare ground, sparse vegetation, forested	Bare ground	Sparse vegetation	Forested	Densely forested areas would be impacted by developing a GHE borefield.	https://planning.hawaii.gov/gis/download-gis-data-expanded/
Critical Species Habitat	Critical		No critical species present		Critical species present	It may be possible to install a GHE system and not disturb critical species habitat.	https://planning.hawaii.gov/gis/download-gis-data-expanded/
Restricted Watersheds	Useful/ Critical		Unrestricted		Restricted	With a closed-loop system, deployment of a GHE system might be permitted in a restricted watershed.	https://planning.hawaii.gov/gis/download-gis-data-expanded/
Underground Injection Zones	Useful		Distant		Proximal	There may be competing uses to the subsurface, and injection may perturb subsurface temperatures; these areas may have better subsurface characterization.	https://planning.hawaii.gov/gis/download-gis-data-expanded/
Recycled Water Management Zones	Useful		Unrestricted	Conditional	Restricted	There may be competing uses to the subsurface, and water recycling may perturb subsurface temperatures; these areas	https://planning.hawaii.gov/gis/download-gis-data-expanded/

						may have better subsurface characterization.	
Water Quality	Useful	Water to be left in natural state, discharge allowed, water known to be toxic/corrosive	Discharge allowed	Water to be left in natural state	Water known to be toxic/corrosive	For closed-loop system, main concern would be corrosion to underground installation. Heating of subsurface over time would perturb natural state conditions.	https://planning.hawaii.gov/gis/download-gis-data-expanded/
Existing Wells	Useful					Existing wells may provide useful information regarding subsurface conditions, but may also indicate competing uses of the subsurface.	https://www.higp.hawaii.edu/hggrc/projects/geothermal-digital-collection/groundwater-collections/
Cultural Parameters							
Land Ownership	Useful	Private and public lands	U.S. Department of Defense, UH lands		Some private land, protected land	Landowner needs to provide access to site, some landowners are motivated.	https://planning.hawaii.gov/gis/download-gis-data-expanded/
Schools	Useful	Public and private	School sites			Schools often have significant cooling load, interest in developing renewable energy resources; GHE system provides educational opportunities.	https://planning.hawaii.gov/gis/download-gis-data-expanded/
Parks	Useful		No parks	Urban, multi-use parks	National parks and preserves	Parks often restrict or prohibit development. Also, parks may not have a need for cooling nearby.	https://planning.hawaii.gov/gis/download-gis-data-expanded/

Archeology/ Cultural Site	Critical	No identified sites		Identified sites	Presence of archeological or cultural features would likely preclude GHE deployment.	https://planning.hawaii.gov/gis/download-gis-data-expanded/
Community Heat Index	Useful	High heat index: greater need for resilient cooling		Low heat index: lesser need for resilient cooling	Linked to cooling demand	https://www.arcgis.com/apps/View/index.html?appid=ff1b73d836074cf6b2aca420fffbd930 (for O'ahu)
Population Density	Useful	High density	Intermediate density	Low density	Greater cooling demand with more concentrated population density, impact of urban heat island effect.	https://files.hawaii.gov/dbedt/op/gis/maps/2010_pop_density.pdf
Cooling Demand	Critical	High cooling demand		Low cooling demand	GHE systems in greater need where cooling demand is higher.	https://www.honolulugis.org/

2.4 Considerations for Open-Loop and Seawater GHE Systems

For typical closed-loop GHE systems, the hydrological setting is not considered critical, because heat transfer is assumed to occur entirely, or at least primarily, by conduction. This differs sharply from open-loop systems, where direct use of groundwater requires a detailed knowledge of hydrological conditions. But for our application in Hawai‘i, with small temperature differences between air and groundwater temperatures and a cooling-dominated load, we rely on groundwater flow to sweep heat away from the borefield. Thus, we need the same detailed knowledge of hydrological conditions as required for open-loop systems. One area that does differ between open- and closed-loop systems involves restricted watersheds and water quality, where the direct use of groundwater in the open-loop system provides greater restrictions on development of a GHE system.

For seawater GHE systems, cultural parameters remain largely the same as for closed-loop systems, and ecological and environmental parameters generally have a seawater counterpart, but physical parameters are entirely different. Replacing geology and hydrology is access to cool seawater temperatures. Economic access relies on the temperature-depth profile of the seawater being steep enough so that cool temperatures can be reached without excessive piping. Physical restrictions on access such as cliffs and especially rough ocean conditions also must be considered.

2.5 Favorability Maps

Table 1 above represents our initial list of screening parameters for closed-loop GHE. When we started to implement this in practice, we found that the large number of parameters was cumbersome, and that not all the datasets were available, so a simplified list of parameters was developed, as shown in Table 2. This list applies for both closed-loop and open-loop systems, and there is only one distinction between the two, regarding inland water quality. GIS maps of individual parameters are shown in Appendix A.

Figure 2 and Figure 3 show the O‘ahu overall favorability maps for closed-loop and open-loop GHE systems, respectively. Each parameter is defined on 500 by 500 m pixels, with a rank of 1, 2, or 3, denoting unfavorable, somewhat favorable, or favorable, respectively. Then the ranks for each parameter at each pixel are added up to produce the overall favorability map. Thus, the higher the overall rank for a given pixel, the more favorable the location. With 10 categories, the highest overall rank possible would be 30, and the lowest would be 10. One exception to the 1, 2, 3 ranking is that for open-loop systems, there is a “do not proceed” rank of -100 applied to the Inland Water Quality parameter where groundwater must be left in its natural state. It is clear from comparing Figure 2 and Figure 3 that this restriction on water quality has a large impact on the overall favorability maps, but both maps show notably high favorability in several coastal areas (Ewa, Maili, Haleiwa, Kahuko, Kaneoho, and Honolulu) as well as the upland area of the O‘ahu North Shore.

Favorability maps in themselves do not tell the whole story. There are four overlays that can be added to augment the analysis, as shown in Figure 4–Figure 7 for the closed-loop favorability map. Figure 8–Figure 11 show the same overlays on the open-loop favorability map. The first three overlays show potential customers for GHE systems: the U.S. Department of Defense and Department of Hawaiian Home Lands parcels, public and private school locations, and areas with high population density (defined as urban areas with 5,000 people or more and/or 2,000 housing units). The fourth overlay shows restricted areas where GHE development would not be possible. By combining favorability maps and overlays, we have integrated all attributes of supply, demand, and regulation that go into GHE development.

Table 2. Screening Parameters Used for Closed-Loop and Open-Loop GHE Favorability Maps

Data Type	3 – Favorable	2-Somewhat Favorable	1 – Unfavorable
Elevation	0 - 20 m	20 – 100 m	> 100 m
Land Surface Slope	2 – 5^{o}	5 – 10^{o}	0 – 2^{o} & >10^{o}
Soil Moisture Zones	Very wet	All others	Arid & very dry
Geology	Shield-stage lava, hyaloclastite/breccia, karst limestone	Post-shield-stage lava, non-karst limestone	Alluvium, unfractured basalt
Soil Permeability: Ksat Class	Fast or very fast > 1 m/day	Moderate 0.3 – 1 m/day	Slow < 0.3 m/day
Aquifer Flow Rates	> 10 MGD	< 10 MGD	
Land Use/Land Cover†	12, 13, 16, 17	22, 24	11, 14, 31, 32, 33, 42, 53, 54, 61, 62, 75, 76
Underground Injection Zones	Below (Makai)		Above (Mauka)
Recycle Water Mgt Zones	No restrictions	Conditional	Restricted
Inland Water Quality - Closed Loop*	Discharge allowed	Waters left in natural state	
Inland Water Quality – Open Loop*	Discharge allowed		Waters left in natural state (-100)**

†See Appendix A for meaning of numbers

*Inland Water Quality was binned two different ways but only one layer was used at a time depending on whether the assessment was for a Closed Loop or Open Loop cooling system.

**These data were considered ‘Do Not Proceed’ in these zones and were given large negative values to highlight those locations.

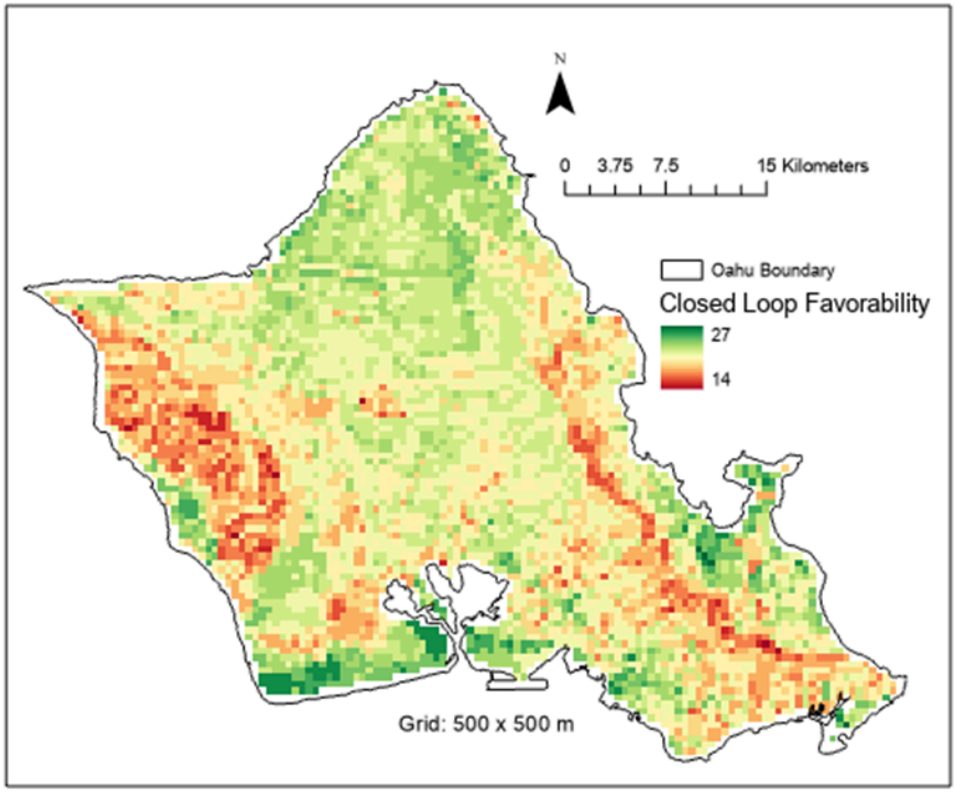

Figure 2. Favorability map for a closed-loop GHE system

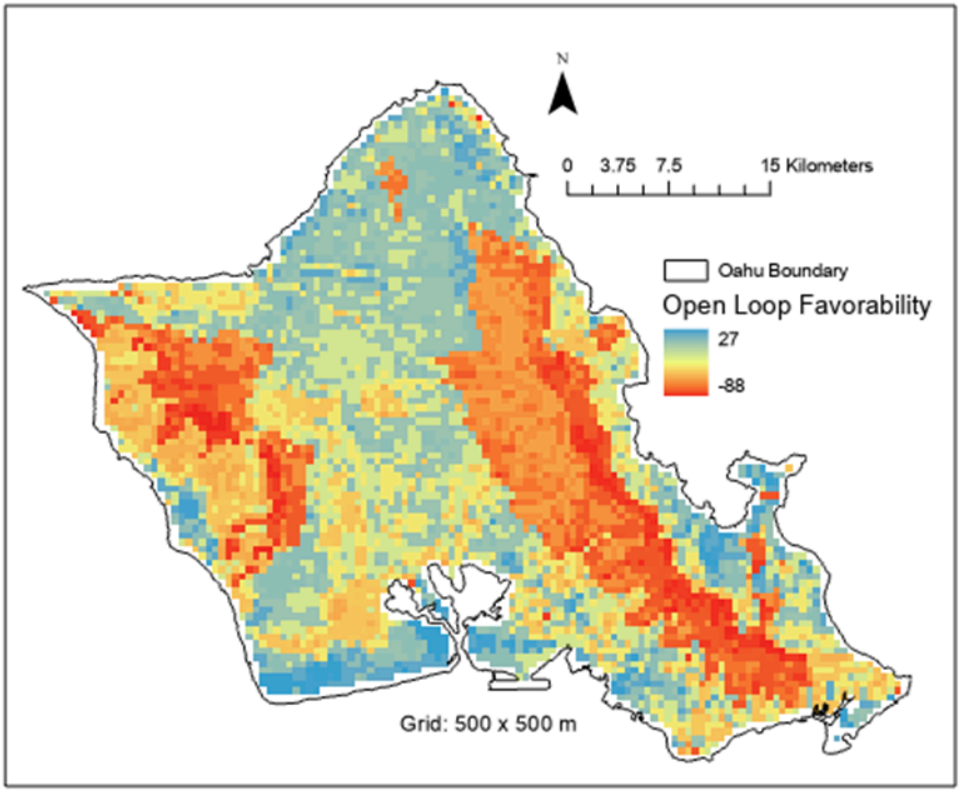

Figure 3. Favorability map for an open-loop GHE system

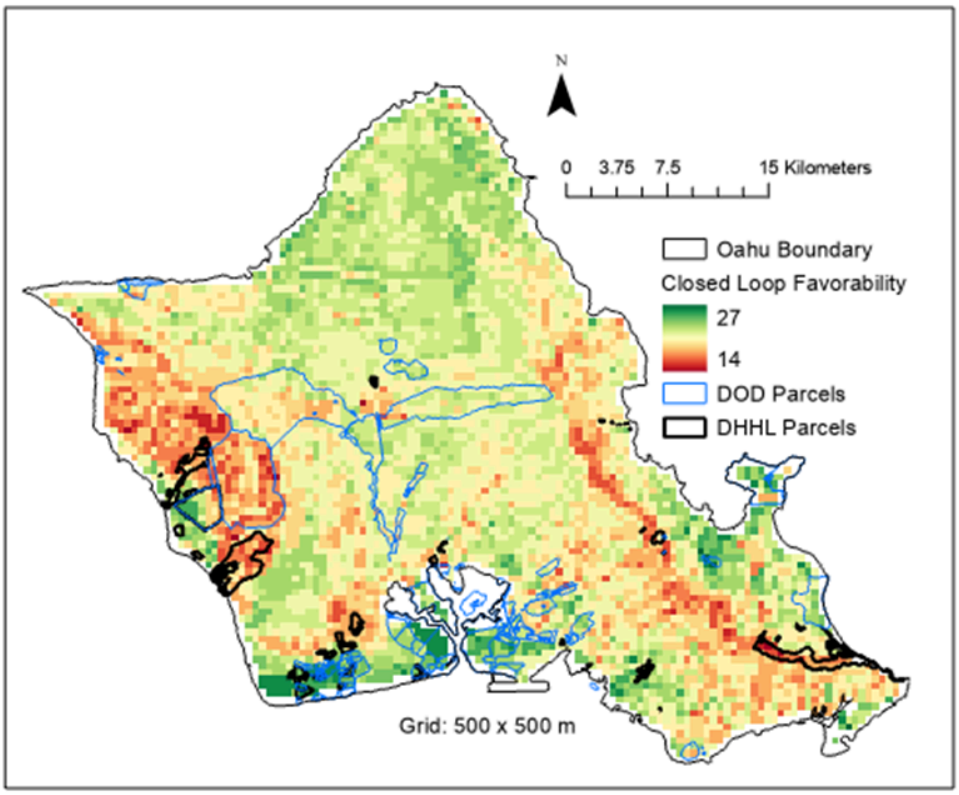

Figure 4. Closed-loop favorability map with U.S. Department of Defense and Department of Hawaiian Home Lands parcels identified

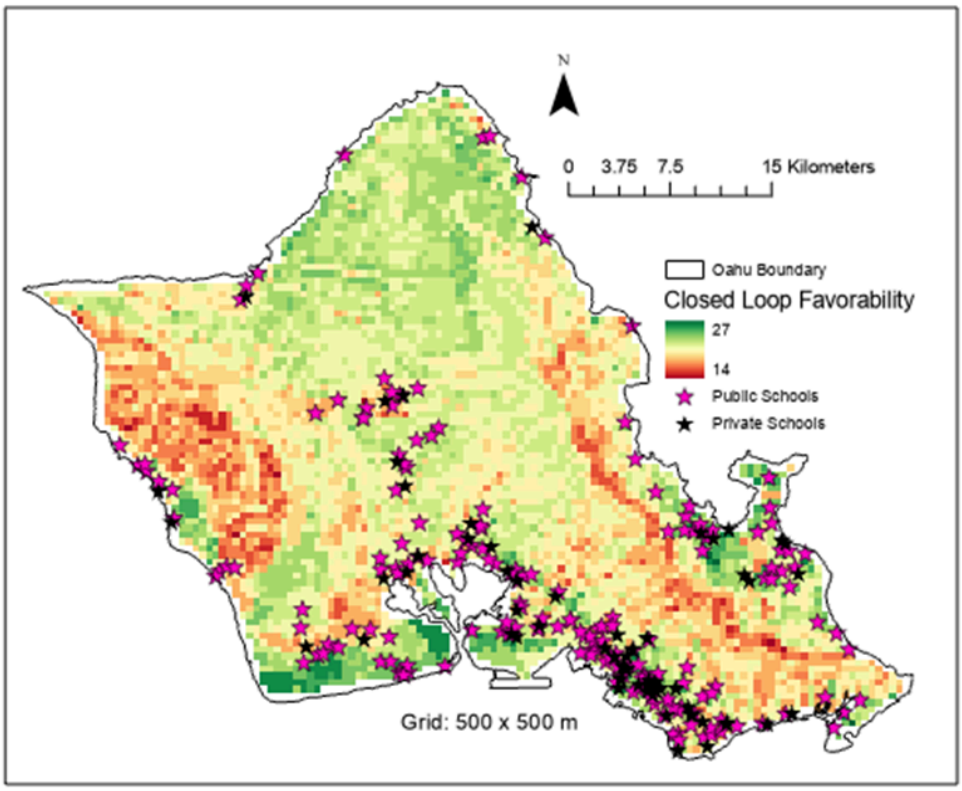

Figure 5. Closed-loop favorability map with public and private school locations identified

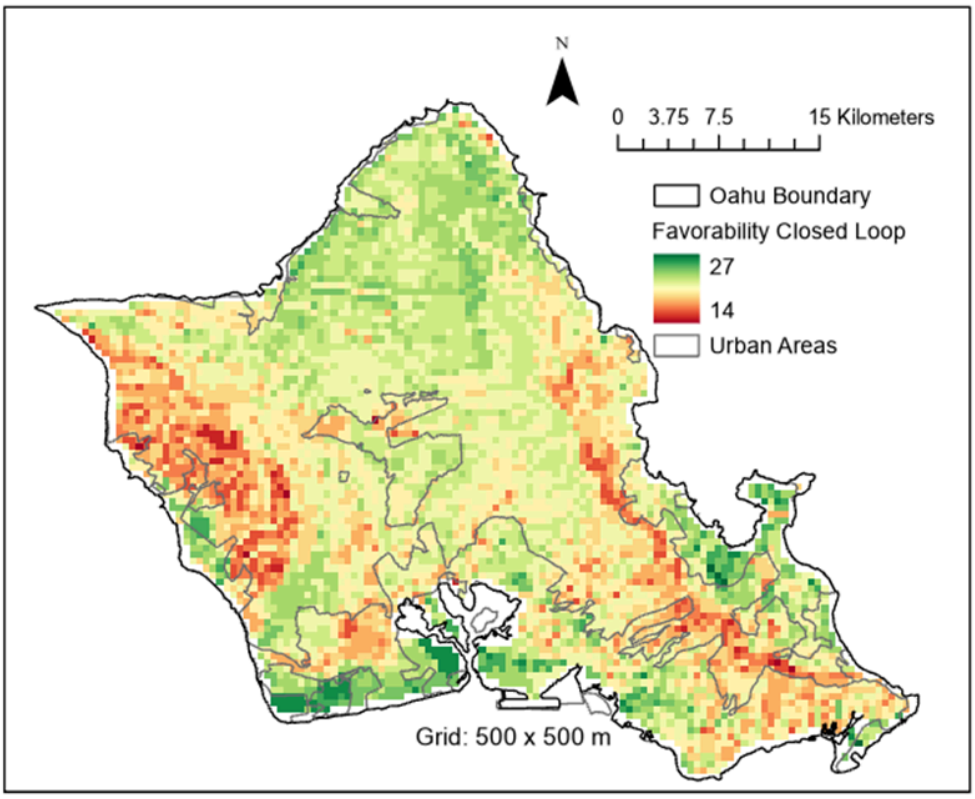

Figure 6. Closed-loop favorability map with areas of high population density identified as urban

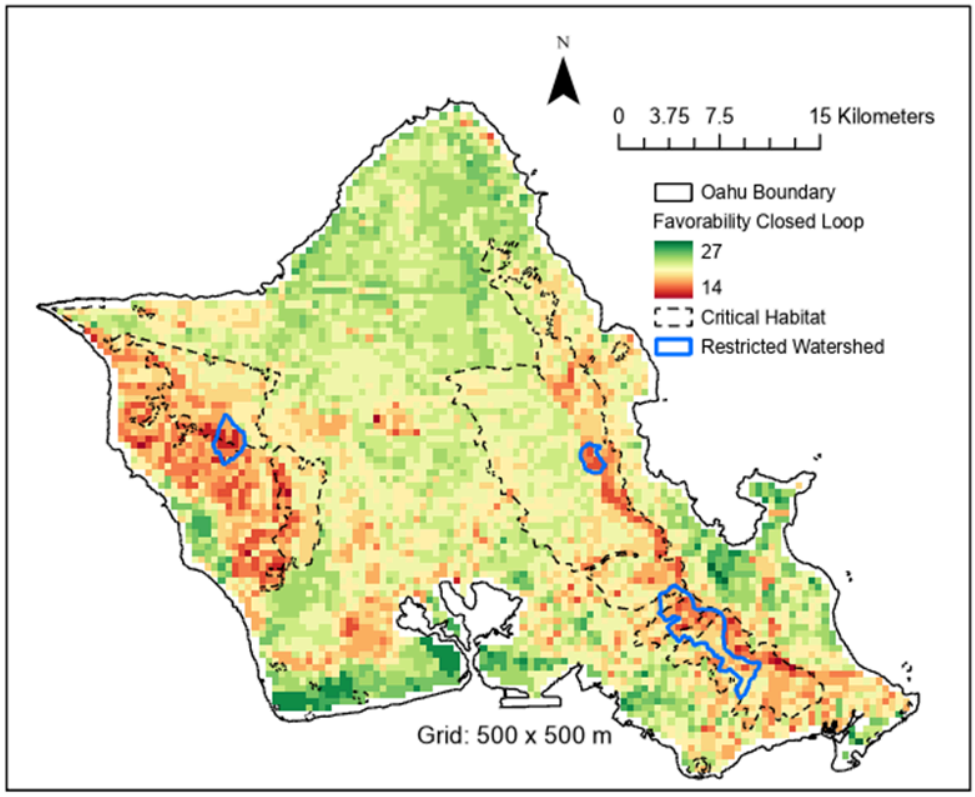

Figure 7. Closed-loop favorability map showing restricted areas where GHE development is not possible

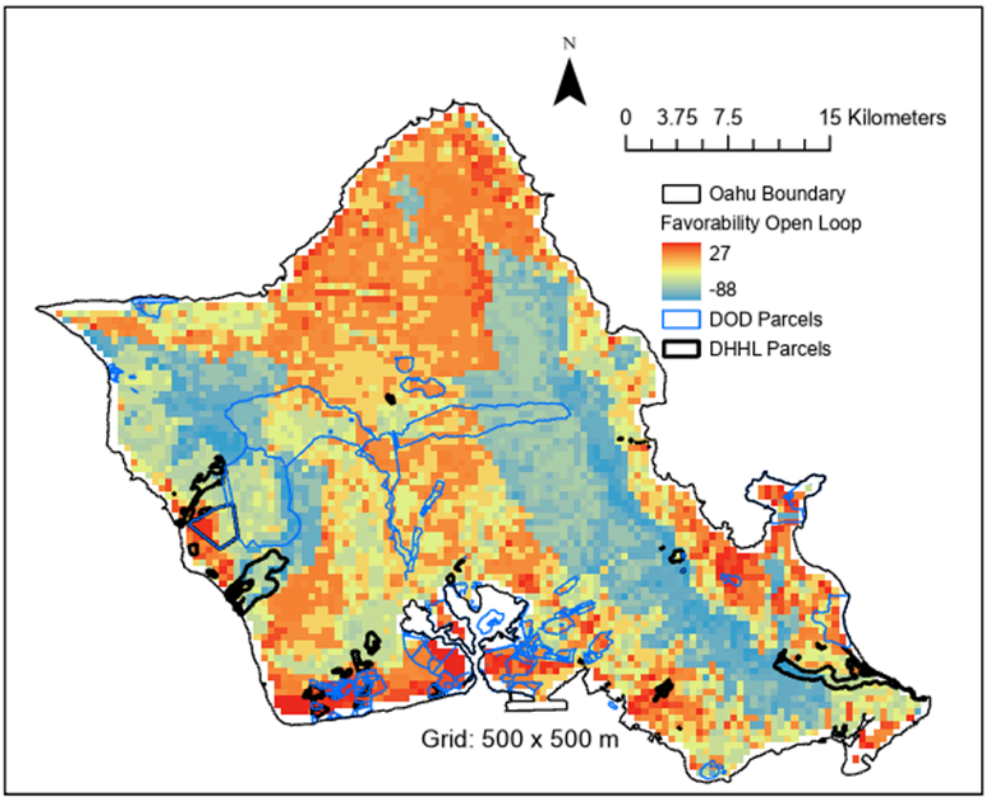

Figure 8. Closed-loop favorability map with U.S. Department of Defense and Department of Hawaiian Home Lands parcels identified

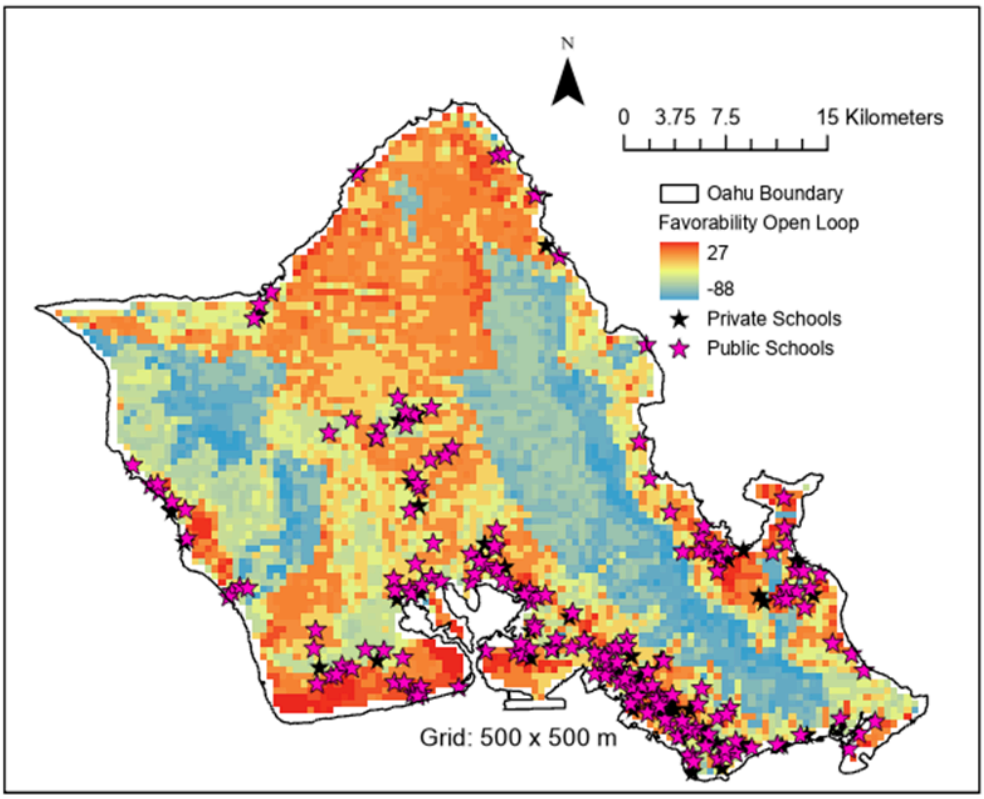

Figure 9. Open-loop favorability map with public and private school locations identified

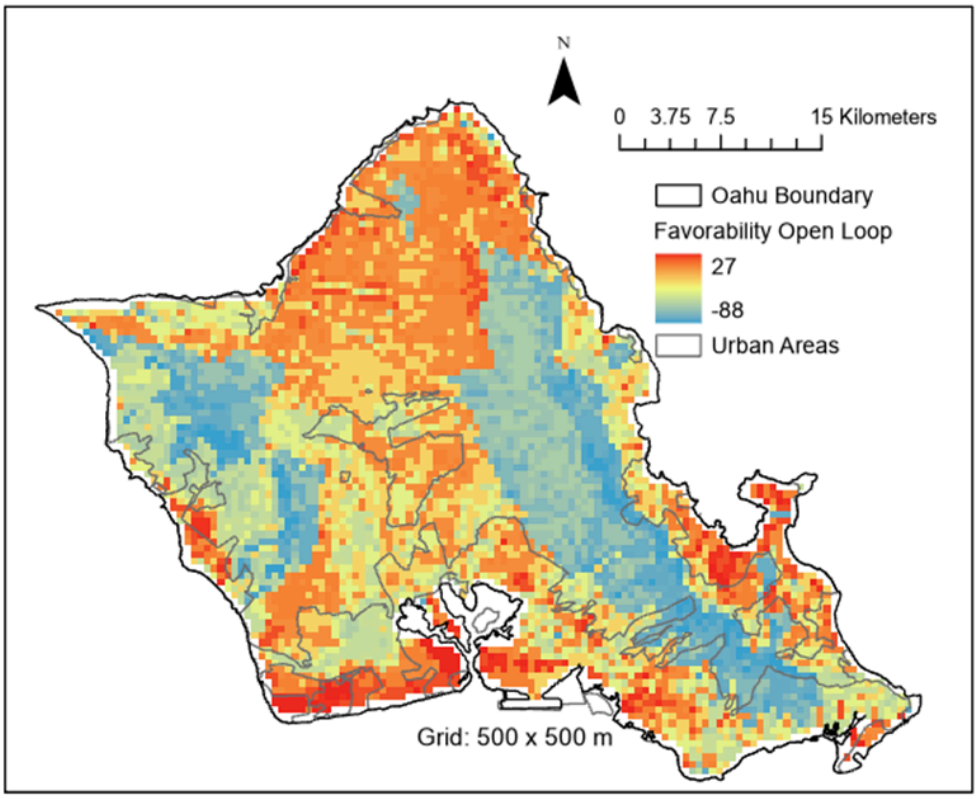

Figure 10. Open-loop favorability map with areas of high population density identified as urban

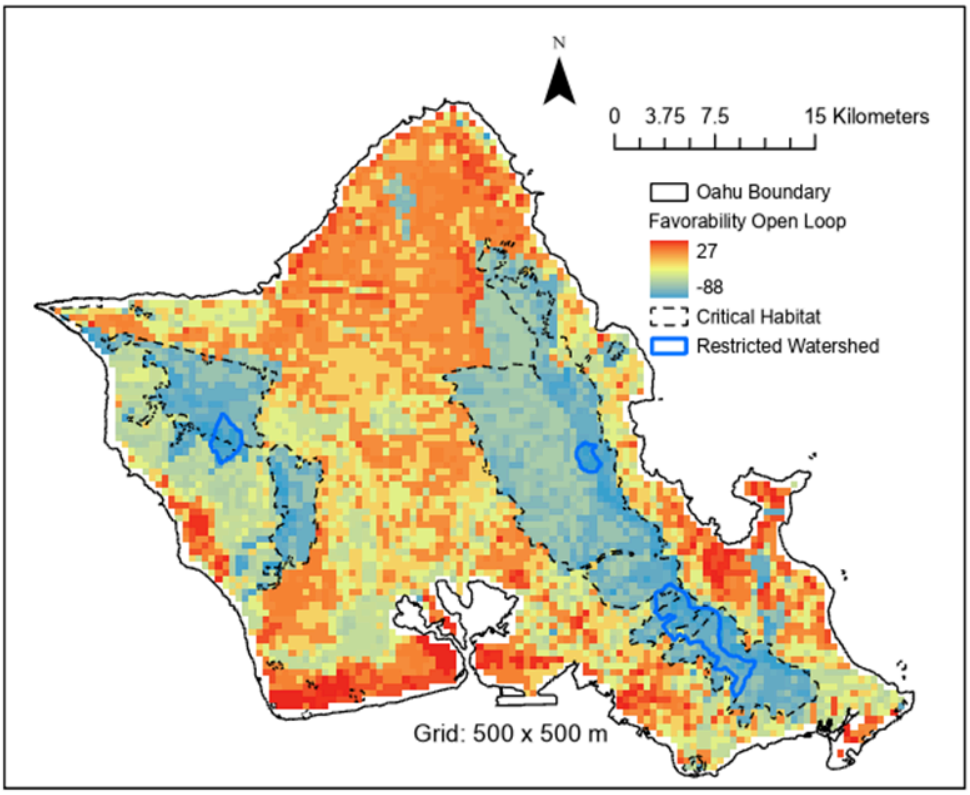

Figure 11. Open-loop favorability map showing restricted areas where GHE development is not possible

3. Targeted Sites

Table 3 shows the candidate sites we considered for doing a detailed GHE analysis, along with some salient features of each site, including geographic/geologic setting, surface elevation, the kind of demand present, the availability of building and subsurface data, and any special features.

It is interesting to contrast the style and content of Table 2 and Table 3. There is quite a bit of overlap in content, but Table 2 is a more general screening tool and Table 3 compares the attributes of specific sites.

All of the candidate sites have high demand for cooling, and at least some argument for why a GHE would be successful, either highly permeable rock that would enable groundwater flow to sweep excess heat away from the borefield, or a very cold source of fluid. The amount of building and subsurface data available varies widely among sites, and is a key factor in determining our final choice: the Stan Sheriff Center on the UH Manoa campus, where a karstic limestone overlies a highly fractured basalt, where we have actual load data for more than a year, as well as a number of sources of geologic and hydrologic information.

Table 3. Candidate Sites Considered for GHE Analysis

Geographic/ Geologic Setting (Island)	Candidate Sites	Elevation (masl)	Kind of Demand	Building Data Availability	Subsurface Data Availability	Special Features
			Favorites			
Ewa Plain (O‘ahu)	UH West O‘ahu, Department of Hawaiian Home Lands offices, hotels	41	Hotel and school building cooling	Good for UH buildings	Good	UH West O‘ahu already has central chiller connected to all buildings, plenty of open space for borefield.
Saturated Karst Overlying Basalt (O‘ahu)	Stan Sheriff Center, UH Manoa athletics complex	5	Cooling of large basketball arena and smaller training facilities	Good; have in spreadsheet form	Good, multiple studies cover area	Limited open area for borefield. Possibilities: sports fields, H1 cloverleaf
Saturated Basalt (Hawai‘i)	Hilo airport	15	Terminal building cooling; cold storage	Unknown	Very cold ocean water (~8°C) at 600-m depth; good stratigraphic data from Hawai‘i Scientific Drilling Project	Possibly good access for drilling in open land; possibility to coordinate with wastewater treatment plant
Moist Vadose Zone, Basalt (Hawai‘i)	Komohana Research Complex, UH Hilo	99	Laboratory building cooling	Good; have in spreadsheet form	Unknown	Dissatisfaction with current cooling method; high rainfall could make vadose zone wet enough.
			Others			
Higher Elevation With Unsaturated Basalt (O‘ahu)	Kamehameha school campus; Tripler hospital	75 to 230	School and hospital building cooling	Limited	Unknown	Thermal conductivity could be prohibitively low.
Coconut Island (O‘ahu)	UH Institute of Marine Biology	0.30	Cooling of lab buildings, education center, dorms	Some info, but limited	Unknown	Boat-only access, seawater cooling, solar

Geographic/ Geologic Setting (Island)	Candidate Sites	Elevation (masl)	Kind of Demand	Building Data Availability	Subsurface Data Availability	Special Features
Thick (~100-m) Rejuvenation Flow With Saturated Karst Below (Oʻahu)	UHM main campus	30	Cooling of multistory buildings with labs, and/or smaller areas	Good	Cross-section of thick flow is visible.	Higher hydraulic head, no connection to ocean
Tidal Slush Zone (Oʻahu)	Waikiki hotels	0	Hotel building cooling	Unknown	Limited; stratigraphic section of caprock	Huge demand
Kona Coast, Very Permeable Subaerial Basalt Lava Flows (Hawaiʻi)	UH Palamanui	140	School building cooling	Good	Good, from recent Ph.D. theses	Newish campus, surrounding area is not built out. Groundwater may be too deep.
Kona Coast, Very Permeable Subaerial Basalt Lava Flows (Hawaiʻi)	Kona Airport	1 to 9	Terminal building cooling	Unknown	Unknown	Cold seawater currently being used for office building cooling; feasibility being prepared for cold water well.
Saturated Basalt, Gigawatt Discharges Subsea (Hawaiʻi)	Offshore Hilo	0		Unknown	Data from deep boreholes drilled for Hawai'i Scientific Drilling Project	Big delta T, users of GHE would be onshore.

4. Evaluation of the Stan Sheriff Center at UH Manoa

We identified the Stan Sheriff Center at the UH Manoa campus as the best candidate to evaluate for cooling using GHE technology. It has a very high cooling load and is surrounded by open space and athletic fields where GHEs could be deployed. We have actual load data for more than 1 year. The following sections describe our efforts on three fronts to evaluate the potential for this area to sustainably provide cooling using a GHE. In Section 4.1, we develop a subsurface thermo-hydrological model to examine coupled groundwater and heat flow using the Transport of Unsaturated Groundwater and Heat simulator (TOUGH); in Section 4.2, we develop an integrated model of the entire GHE system with a simplified no-groundwater-flow model of the subsurface using the Modelica Building Library; and in Section 4.3, we do an economic analysis of a GHE system using inputs from both TOUGH and Modelica results.

4.1 Subsurface Modeling With TOUGH

The numerical simulator TOUGH (Jung et al. 2018) is a multi-phase, multi-component simulator for fluid flow and heat transport through porous or fractured geologic media, which was used with Equation of State module EOS1, which considers one mass component (water) and the transport of heat. Subsurface modeling includes characterization of the local geology and hydrology in order to develop a 3D hydrogeologic model, creation of a numerical model including grid construction and property assignment, running hydrologic simulations to establish initial conditions for the GHE system, then running thermo-hydrologic simulations of the GHE system itself.

4.1.1 Geologic Model of the Stan Sheriff Center Site

A variety of data sources were used to create a 3D geologic model of the area surrounding the Stan Sheriff Center at the UH Manoa campus (Wolf 1975; Finstick 1996; Halliday 1998; Clague et al. 2016; Okuhata 2017; Sherrod et al. 2021). The campus is partially located in an old quarry within the 76-ka Sugarloaf melilite nephelinite flow, which is reported to have a thickness of 15 m (Clague et al. 2016). A series of limestone underground caves have also been reported in the area (Halliday 1998). Limestone reef deposits outcrop just seaward of the campus, on the south side of H1 (Figure 12). Just to the north is Waʻahila Ridge, representing a series of older lava flows from the Koʻolau volcano. A number of engineering geology borings in the area help constrain the shallow subsurface geology as well as the depth to the water table, which is generally around 2.4 m to 3 m (8 ft to 10 ft) depth below ground surface. All of this information was georectified and imported into the Leapfrog 3-D geologic modeling tool. Figure 13 displays the plan view image of the study site, as well as a cross-sectional view of the area. For simplicity, six geologic units were identified: the older Koʻolau basalt (which forms the basement rock of this area), the younger Sugarloaf lava flow, limestone, coralline sand, alluvium, and fill. The locations of identified shallow limestone caves are also represented in this geologic model.

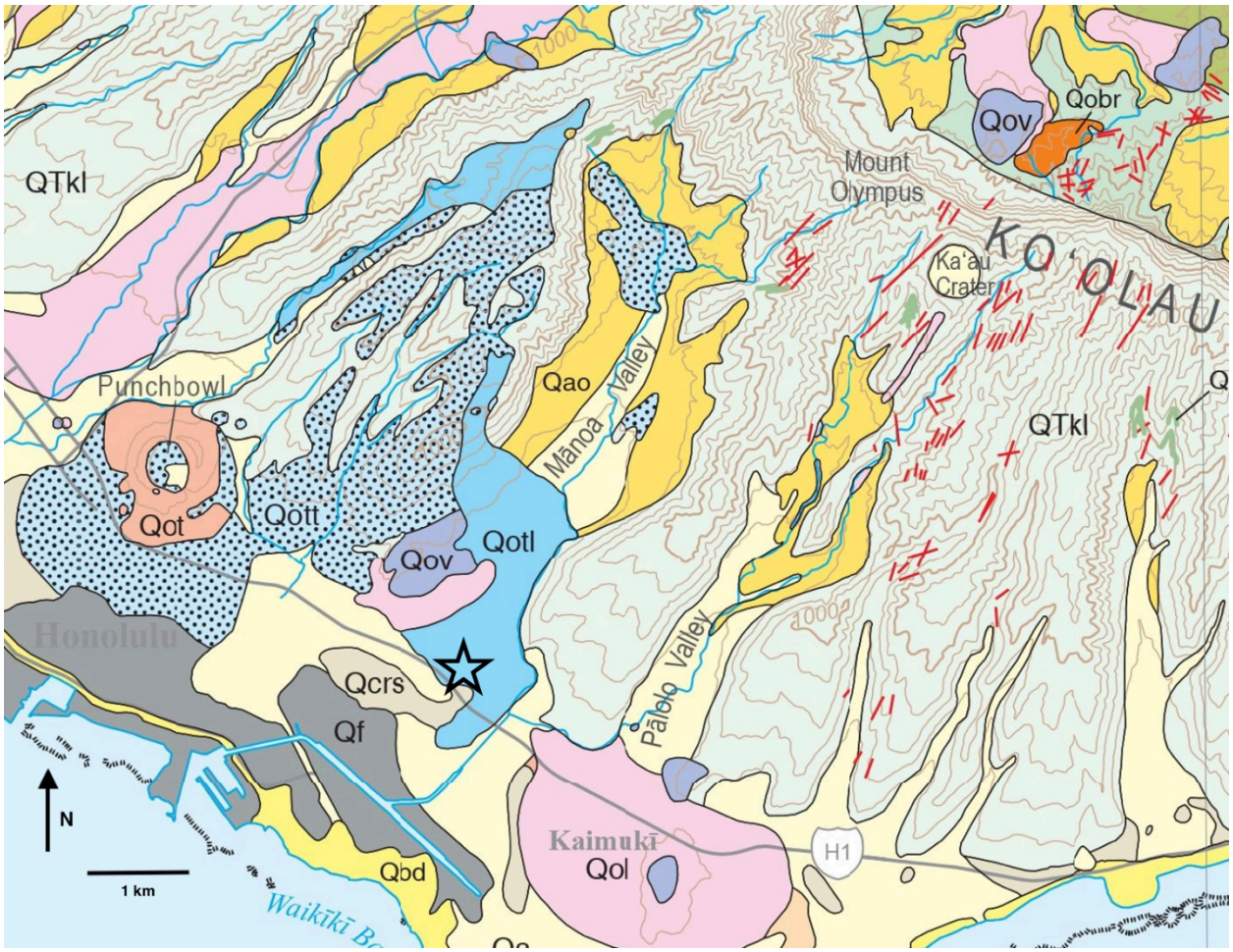

Figure 12. Portion of the geologic map featuring southern O‘ahu, from Sherrod et al. (2021). Depicted geologic units are as follows: Qf - Fill (Holocene); Qa - Alluvium (Holocene and Pleistocene); Qao - Older alluvium (Pleistocene); Qbd - Beach deposits (Holocene); Qcrs - Calcareous reef rock and marine sediment (Pleistocene); Qol - Lava flows, Honolulu Volcanics (Pleistocene); Qov - Cinder vent deposits, Honolulu Volcanics (Pleistocene); Qot - Tuff cone deposits, Honolulu Volcanics (Pleistocene) Qotl - Lava flows from Tantalus Peak and Sugarloaf vents, Honolulu Volcanics (Pleistocene); Qott - Tuff from Tantalus Peak and Sugarloaf vents, Honolulu Volcanics (Pleistocene); QTkl - Lava flows from Ko‘olau Basalt (Pleistocene and Pliocene). The star denotes the location of the Stan Sheriff Center at the UH Manoa campus.

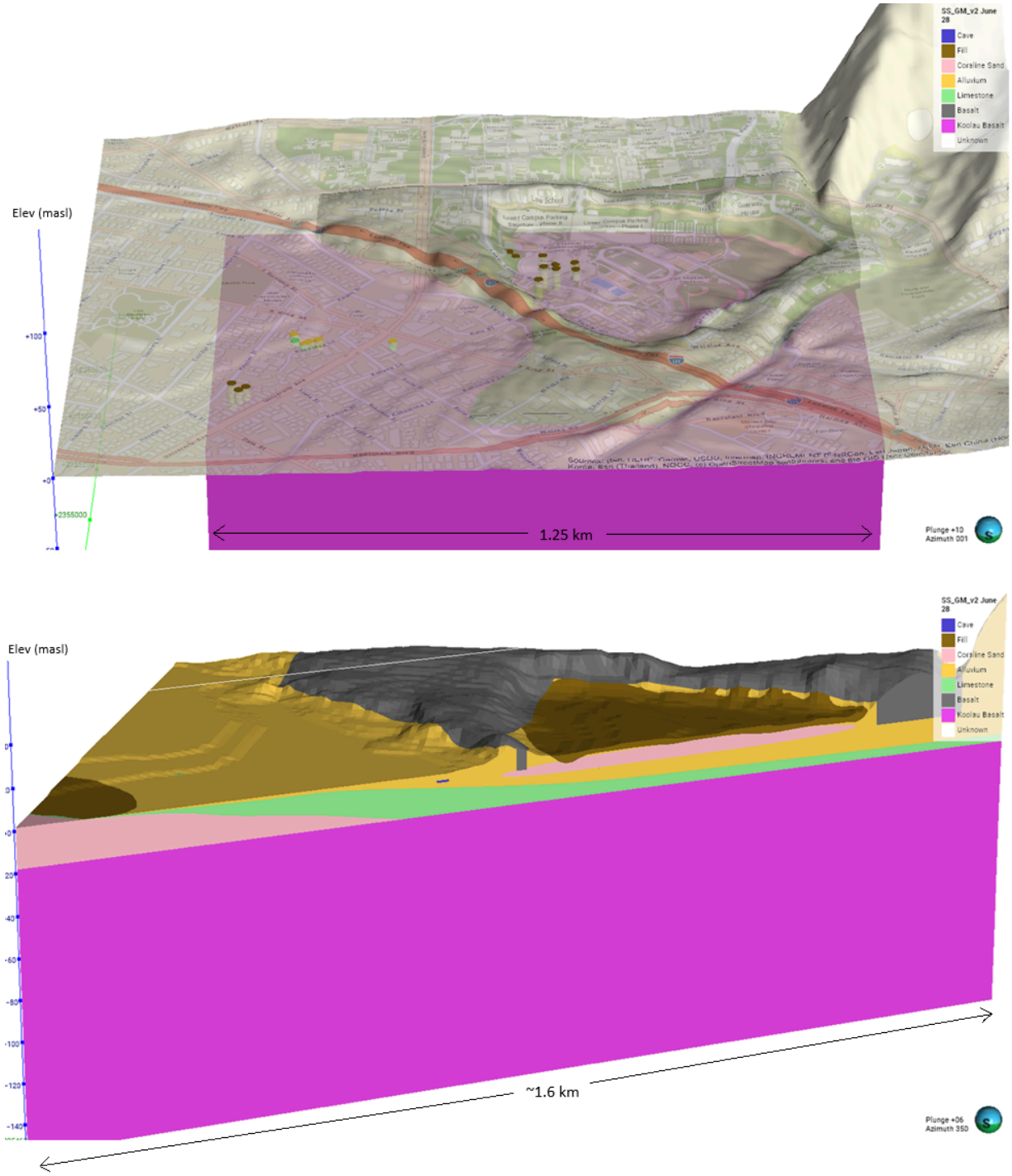

Figure 13. Three-dimensional images from the geologic model of the UH Manoa Stan Sheriff Center. The upper figure shows the excavated quarry in the Sugarloaf lava flow where the athletic complex is located, along with locations of engineering boreholes. The lower figure depicts a cut section through the 3D geologic model, with the exposed cross-section parallel to the main hydrologic flow direction (from right to left). Note that the majority of the geologic section is composed of the older Koʻolau basalt flows. Both figures have an exaggerated vertical scale to help highlight topographic variations.

4.1.2 Hydrogeologic Model of the Stan Sheriff Center Site

At a regional scale, groundwater flows down from the crest of the Koʻolau Range toward the coastline in a southwesterly direction (Nichols et al. 1996) (Figure 14).

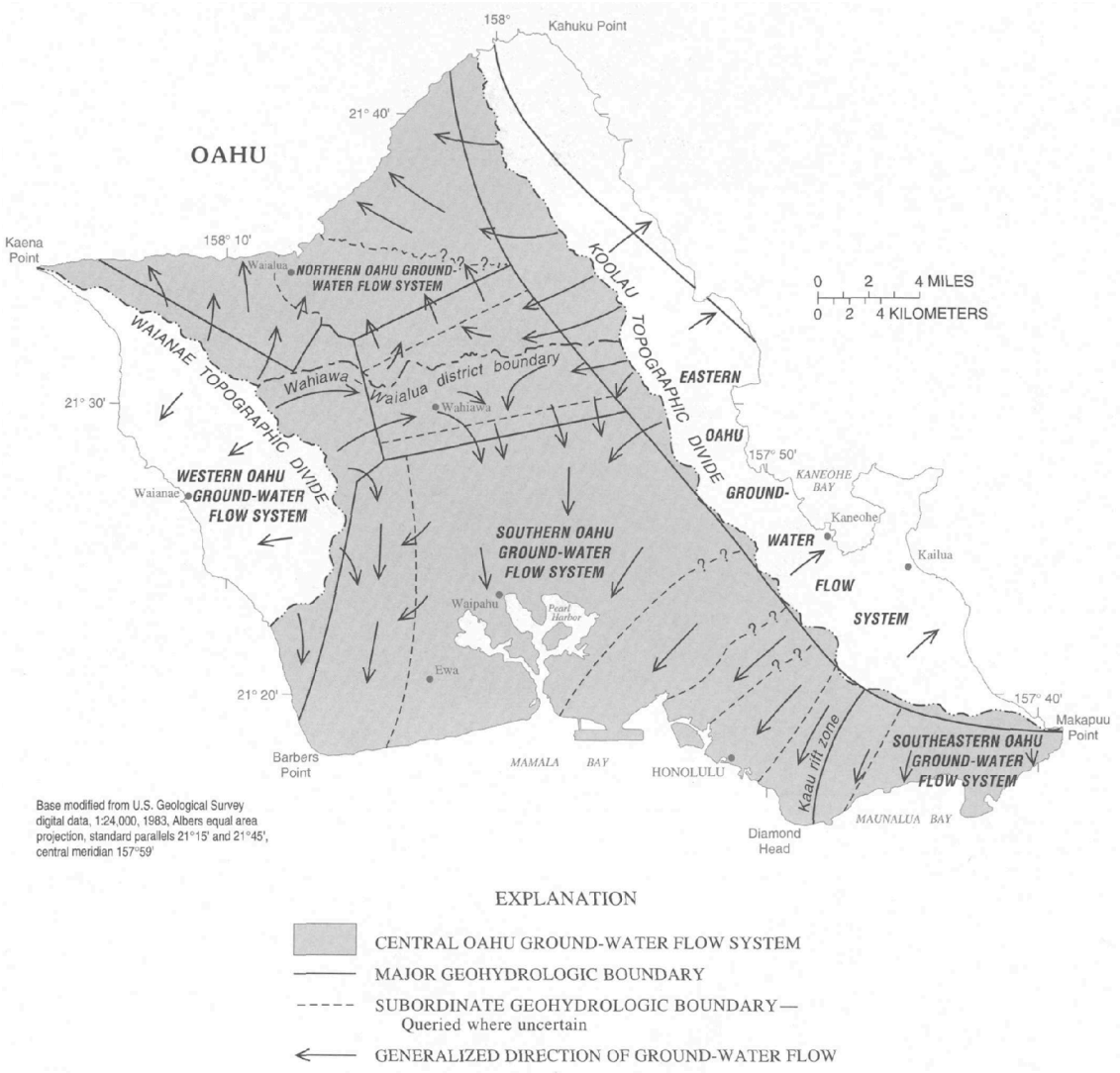

Figure 14. Groundwater flow systems for Oʻahu (Nichols et al. 1996). The UH Manoa campus is located within the southern Oʻahu groundwater flow system, just west of the Kaau rift zone.

Figure 15 shows ground surface elevation, water table elevation, and water table depth for 20 wells in the region surrounding the Stan Sheriff Center. The water table elevation data may be used to infer the direction and magnitude of the hydraulic gradient driving groundwater flow at the Stan Sheriff Center site. The sparsity of the data, and the fact that water level measurements were taken at various times between 1901 and 2024, introduces uncertainty. At three wells, water level transients from 2014–2024 are available, and indicate that water level variability over that time frame was about 1.5 m. Thus, when comparing measurements in Figure 15, differences less than 1.5 m should not be considered significant. Using water table elevations in three wells in the vicinity of the Stan Sheriff Center that follow a transect from mountain to ocean yields a hydraulic gradient of 0.0053. This is quite a bit larger than the regional hydraulic gradient of 0.0002 associated with the

groundwater areas of the central O‘ahu flow system (Oki 1998), and a typical gradient of 0.000262 for the Honolulu Aquifer (Liu 2007), which was also generally used for basalt, limestone, and alluvium for the Hawaiian Islands (Dores and Lautze 2020).

Note that we are considering a shallow GHE system (boreholes only 100–150 m deep) and interactions with the surface (precipitation, evaporation, and infiltration of excess irrigation) and other groundwater users through wells may significantly alter groundwater flow magnitude and direction. These effects are not included in the present report.

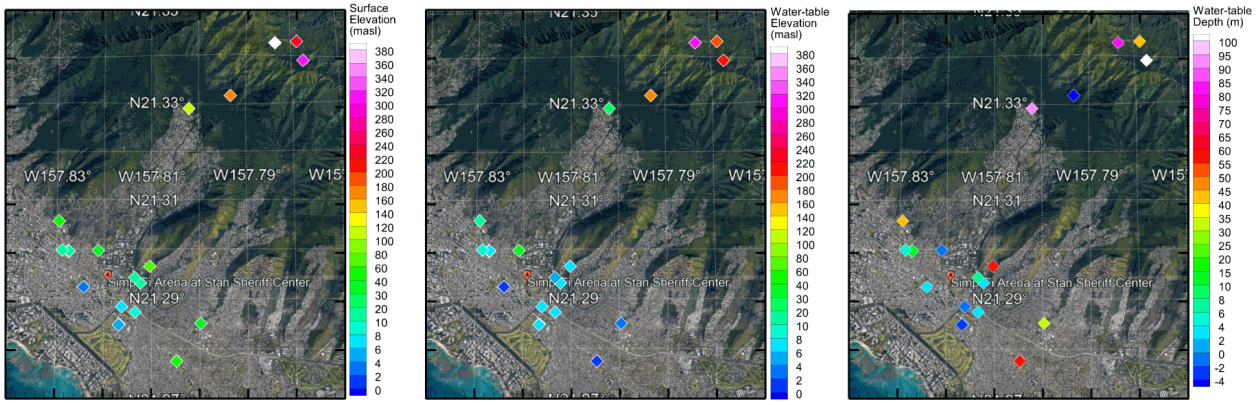

Figure 15. Left: ground surface elevations at 20 well locations. Middle: water table elevations. Right: water table depth below ground surface. The location of the Stan Sheriff Center is shown as a red pin. Note that the contour intervals are non-uniform to enable variations to be observed in both the lowland near the ocean and the highland in the mountains.

4.1.3 Numerical Model Grid

One of Leapfrog’s capabilities is to convert the 3D geologic model into a grid for the numerical simulations, where the grid blocks are assigned the appropriate petrophysical, thermal, and hydrologic properties corresponding to those pertaining to the units in the geologic model (e.g., Milicich et al. 2015). The grid was oriented so that the grid blocks would be parallel to the primary groundwater flow direction, which is northeast to southwest, which enables more accurate computation of groundwater flow and the accompanying heat transfer. The grid extent and thickness were designed to contain the potential region where a GHE system would be potentially deployed for cooling the Stan Sheriff Center. The grid extends from the ground surface (maximum elevation 26 m) to a depth of 565 m. It contains 70 layers, with variable layer thickness ranging from 1 m (z = 26 to z = -20 m), to 10 m (z = -20 to z = -150 m), to gradually increasing thickness to z = -565 m. The upper 26 layers are incomplete, representing the variable surface elevation. The lower 44 layers all contain 3,299 grid blocks. The total number of grid blocks in the model is 164,196. Lateral grid spacing is 25 m, but the central portion of the grid is refined to 12.5 m, to better resolve caves and the borefield. The lateral extent of the model is about 1.3 km in the east-west direction and 1 km in the north-south direction. Although the model itself is oriented east-west/north-south, the grid is rotated laterally to align with the regional groundwater flow direction from northeast to southwest. Figure 16 shows the grid.

The GHE consists of 100 boreholes, each 100 m deep, arranged in a 10 by 10 square array, plumbed in parallel, so that the total flow rate of the above-surface loop is split into 100 equal parts. Typical borehole spacing for GHE is 6 m, but here a 12.5-m separation between boreholes is used in recognition of the unbalanced cooling-dominated load, to provide greater capacity for dissipating waste heat. We do not model the details of the GHE within each borehole (a u-tube embedded in grout), or make a highly resolved radial

grid representing the region around each borehole, but make use of the flexibility of the Integral Finite Difference Method employed by TOUGH for spatial discretization, which allows boreholes to be represented in a simple way following the approach of Falta et al. (2023). Specifically, one new "extra grid block" is introduced to represent each borehole. Because the grid spacing is the same as the borehole spacing, every original grid block column within the footprint of the GHE has one extra grid block associated with it. Each extra grid block is 100 m long and connected laterally to all the grid blocks of the original grid block column over that 100-m interval. The parameters of these lateral connections are specified in a particular way so that the details within the borehole and the radial geometry for heat transfer outside the borehole are represented. In the Integral Finite Difference Method, each connection between two grid blocks requires four parameters to be specified: the distances d_1 and d_2 from the nodal point of each grid block to their common interface, the area A of the interface, and the orientation of the interface with respect to gravity. Here, we specify:

$d_1 = 2 \pi \lambda r_w BTR$

$d_2 = r_w \ln(r_e/r_w)$

$A = 2 \pi r_w \Delta z$

$\beta = 0$ for horizontal connections,

where λ = 2.182 W/m/K is thermal conductivity of the grout, r_w = 0.07 m is the borehole radius, BTR = 0.1 is borehole thermal resistance (an integrated representation of the details within the borehole), r_e =0.208·12.5 m = 2.6 m is the effective radius of the original grid block column connected to the extra grid block, and Δz is the thickness of the original grid block. More details of the extra grid block approach may be found in Falta et al. (2023), and more details of the Integral Finite Difference Method may be found in Jung et al. (2018).

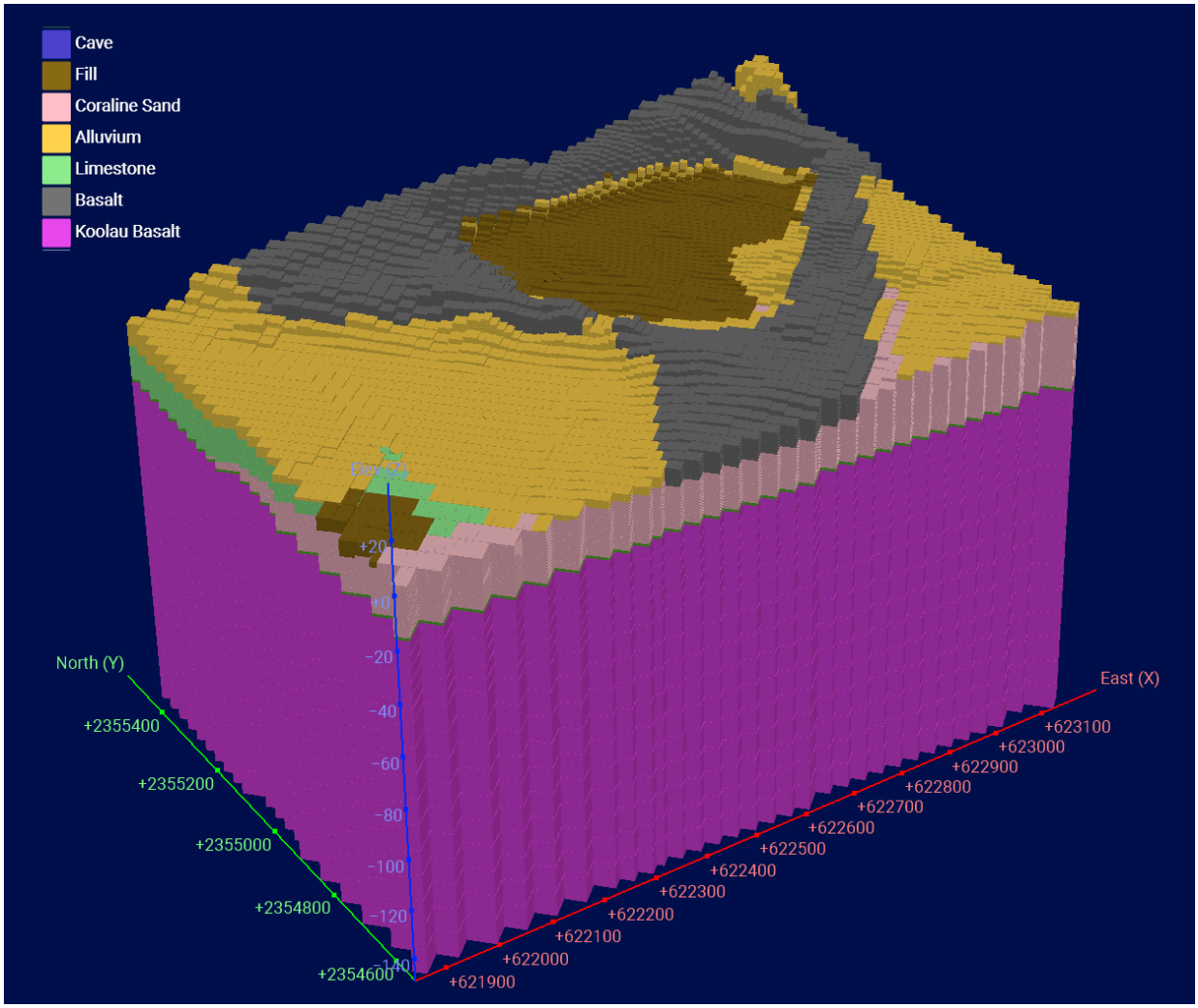

Figure 16. Upper portion of the TOUGH grid used for the preliminary simulations. Note that although the model as a whole is oriented north-south and east-west, the orientation of the rectangular grid is northwest-southeast and northeast-southwest, perpendicular to and aligned with the regional groundwater flow. Axes show distance in meters; vertical exaggeration is a factor of five.

4.1.4 Numerical Model Properties, Initial Conditions, and Boundary Conditions

There have been a number of hydrogeologic studies that have modeled groundwater flow in southern O‘ahu (e.g., Finstick 1996; Nichols et al. 1996; Hunt 1996; Lau and Mink 2006; Rotzoll and El-Kadi 2008; Okuhata 2017; Izuka et al. 2018; Izuka and Rotzoll 2023); they have summarized the hydrologic properties of the main geologic units of this area. In addition, Dores and Lautze (2020) have reported representative thermal conductivity values of the main lithologic units; these have been supplemented by data from Clark (1966) and Robertson (1988). Table 4 and Table 5 present a summary of these properties, which are needed to properly simulate the groundwater flow and heat exchange of a GHE system. It is important to note that if 100-m closed-loop borehole heat exchangers are to be used, then the Ko‘olau basalt unit will be the primary hydrogeologic unit controlling the heat exchange (the geologic model depicted in Figure 13 suggests that this unit will be present at depths greater than 20 m).

Table 4. Summary of Key Hydrologic Properties of Primary Geologic Units

Rock Type	Hydraulic Conductivity K (m/d)	Effective Porosity ϕ (%)	Comments	Sources
Ko'olau Basalt (dike-free lava)	600 (horizontal longitudinal) 150 (horizontal transverse) 0.75 (vertical)		Values used in our simulations	Okuhata (2017)
	152–1,524			Hunt (1996)
	457, 305–1,524	5	Porosity value used in our simulations. Vertical permeability estimated to be much lower than horizontal.	Lau and Mink (2006)
	401–550			Rotzoll and El-Kadi (2010)
Honolulu Volcanics	3 (horizontal longitudinal) 1 (horizontal transverse) 0.05 (vertical)		Values used in our simulations	Okuhata (2017)
	0.3–152			Hunt (1996)
Limestone	100 (horizontal longitudinal) 100 (horizontal transverse) 0.5 (vertical)		Values used in our simulations	Okuhata (2017)
	30–6,096			Hunt (1996)
	0.43–53 (13)	15–45 (35)	Used average porosity value in our simulation. Coral ledge.	Finstick (1996)
Alluvium	0.05 (horizontal longitudinal) 0.05 (horizontal transverse) 0.05 (vertical)		Values used in our simulations	Okuhata (2017)
	0.0009–2.9 (0.9)	38–71 (54)	Used average porosity value in our simulations	Finstick (1996)
	0.006–0.113	46.4–62.4	Values for older alluvium	Lau and Mink (2006)
	0.3–152			Hunt (1996)
Fill	0.015–86 (43)	28–69 (46)	Used average hydraulic conductivity and porosity values in our simulations	Finstick (1996)

Note: Average values shown in parentheses.

Table 5. Summary of Thermal Properties of Primary Geologic Units

Rock Type	Thermal Conductivity λ (W m^{-1} K^{-1})	Specific Heat, C_r (10^3 J/kg K)	Comments	Sources
Basalt	2.0		Value used in our simulations	Dores and Lautze (2020)
	2.1–3.1		Mean values for 2 different lavas measured at 20°C	Clark (1966)
	2.1	1.03	Thermal conductivity determined for non-porous rock with 10% mafic phenocryst content at 300 K; specific heat value for Dresser basalt at 20°C	Robertson (1988)
Limestone	3.1		Value of 3.0 used in our simulations	Dores and Lautze (2020)
	2.18–3.05		Mean values for 3 different limestones measured at 20°C	Clark (1966)
	2.7	1.01	Thermal conductivity determined for non-porous rock at 300 K; specific heat value for Bedford limestone at 20°C	Robertson (1988)
Alluvium	0.8		TC value used in our simulations	Dores and Lautze (2020)

As noted in Table 4, permeability in the basalt is anisotropic, with horizontal permeability much greater than vertical permeability, and longitudinal permeability (i.e., in the direction of the lava flow) higher than transverse permeability. In basalts, permeability is dominated by the presence of fractures. The TOUGH code is able to independently model fracture and matrix permeability by employing a dual continua model, where grid blocks are subdivided into fracture and matrix grid blocks by using the multiple interacting continua (MINC) approach (Pruess 1992). The orientation and spacing of the fracture network can be specified using this approach. For these preliminary simulations, only a single continuum was used, but by orienting the grid with the direction of groundwater flow, we also align it with the orientation of the major fractures, enabling the code to model anisotropic fracture permeability.

Another important input for this model is the initial temperature distribution in the subsurface. There are a number of deep groundwater monitoring wells in southern O‘ahu, including three (Kaimuki High School, Kaimuki Pump Station, and Wa‘ahila) that are fairly close to the UH Manoa campus. As part of the groundwater monitoring effort, multi-parameter sensors that measure fluid electrical conductivity, temperature, and pressure are regularly run in these wells to detect changes in the fresh water-brackish water interface (Rotzoll et al. 2010). The temperature information from these wells, shown in Figure 17, can be used to constrain the general temperature-depth gradient that can be expected for the Stan Sheriff site. For these preliminary simulations a uniform initial temperature of 21.5°C is used, consistent with what Dores and Lautze

(2020) report as an average groundwater temperature (21.36°C) for Honolulu. These temperatures are consistent with the deeper portions of the temperature-depth profiles from the nearby monitoring wells mentioned above that were shared by the Honolulu Board of Water Supply. However, the shallow portions of the profiles show higher temperatures (Figure 17). The shallowest measurements from the profiles are consistent with average air temperatures for the Honolulu area (Figure 18). These temperature-depth profiles suggest a downward flow of warmer water from the surface. The details of the vadose zone and moisture transfer through the ground surface are not addressed in these preliminary simulations, but they are within the TOUGH simulator capabilities and could be included in future modeling. Here, the entire model domain is considered water-saturated, and the top model boundary is held at atmospheric pressure and a temperature of 21.5°C. Previous modeling of shallow GHE with 100-m deep boreholes (Hu et al. 2021) showed that near-surface effects such as a low-thermal conductivity vadose zone and a variable water table had minimal impact on GHE performance. Other boundary conditions specified for the model are a closed bottom boundary and closed lateral boundaries, except at the upgradient and downgradient extremes of the model, where constant-pressure conditions are prescribed to set up a hydraulic gradient to drive groundwater flow, as described in Section 4.1.5.

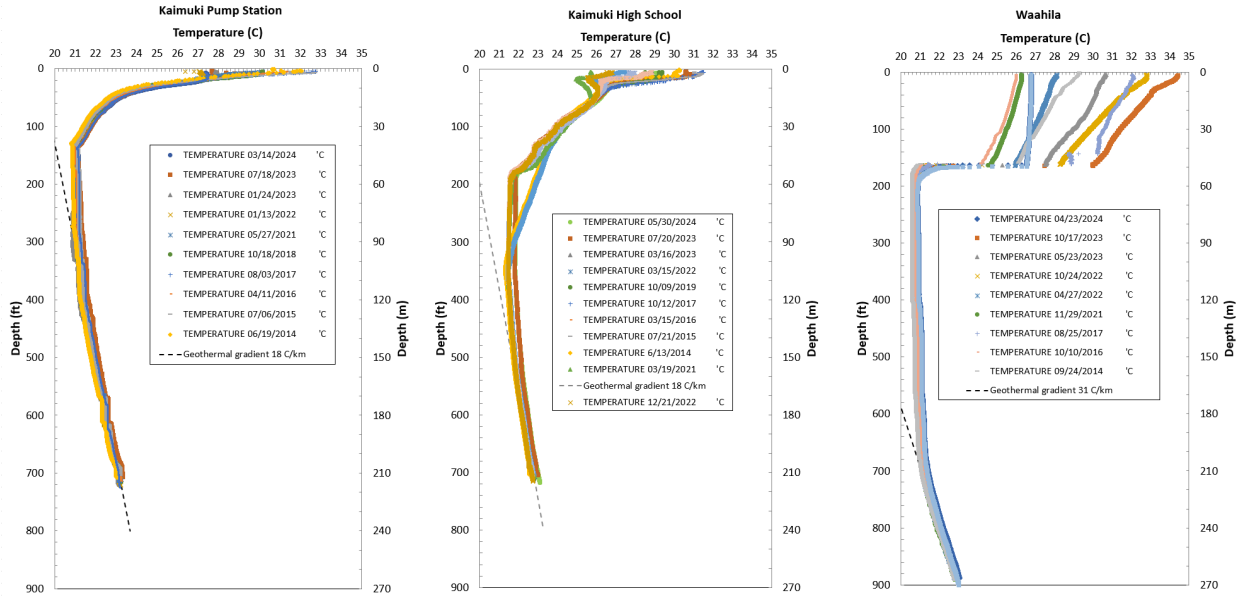

Figure 17. Temperature-depth profiles obtained from monitoring wells at the Kaimuki Pump Station, the Kaimuki High School, and Wa‘ahila, which were obtained between 2014 and 2024. Data courtesy of the Honolulu Board of Water Supply.

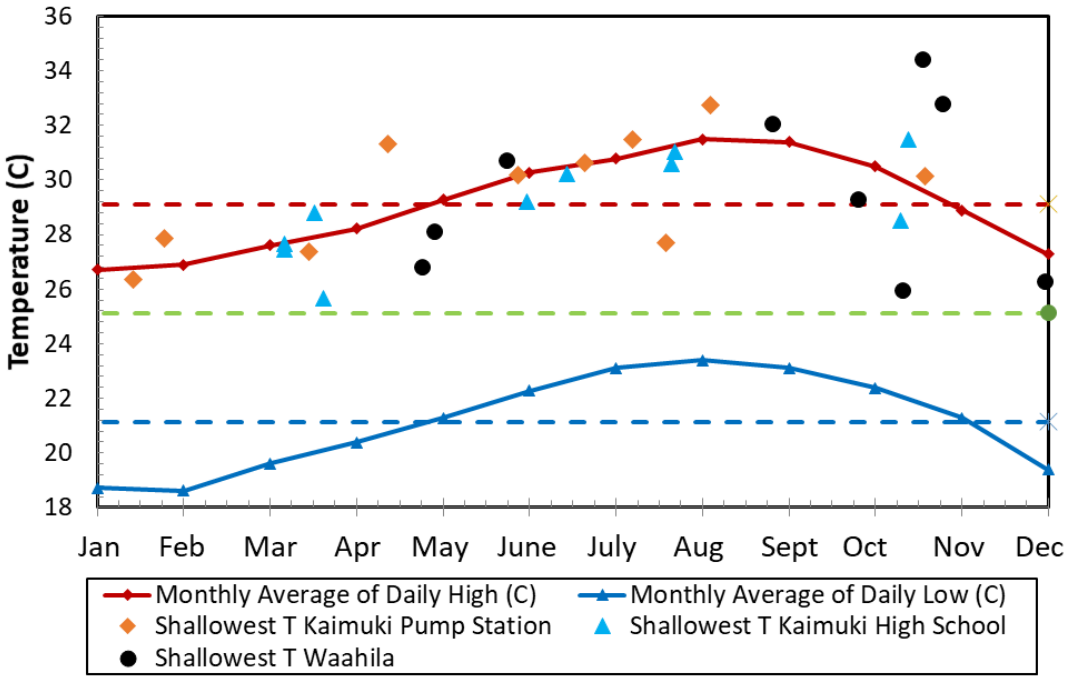

Figure 18. Monthly average high and low air temperatures for Honolulu (solid lines) and annual averages (dashed lines). These are long-term averages, not representative of any particular year. The green dashed line is the average annual temperature. The symbols show the shallowest temperature from each profile from the monitoring wells at the Kaimuki Pump Station, the Kaimuki High School, and Waʻahila, which were obtained between 2014 and 2024.

4.1.5 Hydrogeologic Simulations of the Stan Sheriff Athletic Complex Site To Establish Groundwater Flow Field

Establishing a regional groundwater flow field through the model is a multi-step process. Initially, horizontal permeabilities throughout the grid are set to zero, and a gravity-equilibration simulation is done to create a hydrostatic pressure distribution within each water-saturated grid block column throughout the model, with the uppermost grid block held fixed at atmospheric pressure. Then, horizontal permeabilities are reset to their actual values shown in Table 4, and grid block columns at the upgradient and downgradient extremes of the model are held fixed with at their initial hydrostatic pressure profile, and the model is run to steady state. The elevation difference between the upgradient and downgradient model extremes creates a hydraulic head gradient across the model, driving a regional groundwater flow. The topographic difference between the upgradient and downgradient model extremes is 26 m, and the distance across the model is 1,612 m, yielding a hydraulic gradient of 26/1,612 = 0.016. Of course, this "topographic gradient" assumes that the water table is right at the ground level, which is not the case, as shown in Figure 15. For the modeling studies, we consider four different hydraulic gradients and compare the impact of the resulting groundwater flow on heat transport, as shown in Table 6. Case *A* is the topographic gradient; Case *B* is the gradient calculated from the water levels of nearby wells (Figure 15); Case C is the hydraulic gradient taken from the literature to be typical of southeastern Oʻahu, as discussed in Section 4.1.2 above; and Case *D* is designed to have almost no hydraulic gradient, so heat transport will be by conduction only. Of the four cases, Cases *B* and *C* are the only ones considered to actually represent possible conditions at the Stan Sheriff Center. Cases *A* and *D* are included to further illustrate the effect of groundwater flow. With the extent of the borefield being 125 m, it is expected

that Cases *B*, *C*, and *D* will show rather different effects, as the distance traveled by the thermal plume in 1 year will be much greater than, comparable to, and much smaller than the borefield extent, respectively.

Table 6. Hydraulic Gradients Assumed for Various Cases and the Corresponding Groundwater Velocity and Thermal Velocity Through the Ko'olau Basalt

Case	Hydraulic Gradient I	Groundwater Velocity in Ko'olau Basalt v_{gw} (m/yr)*	Thermal Velocity in Ko'olau Basalt $v_{th} = R \cdot v_{gw}$ (m/yr)**
A. Topographic Gradient	0.016	60,600	4,600
B. Nearby Well Gradient	0.0053	20,100	1,500
C. Literature Gradient	0.00026	992	75
D. ~Conduction Only	0.000016	61	5

*v_{gw} = K I / ϕ, where K = 600 m/day and ϕ = 0.05

**R = $\rho_w C_w \phi / [\phi \rho_w C_w + (1-\phi)\rho_r C_r]$ = 0.076 (where $\rho_w C_w$ = 4.2E6 J/m^3/K and $\rho_r C_r$ = 2.7E6 J/m^3/K are water and rock volumetric heat capacities, respectively)

Because groundwater flow is proportional to the product of permeability and hydraulic gradient, we can use the topographic gradient and decrease the longitudinal permeabilities in the model to produce the groundwater flow resulting from the other gradients. Thus, longitudinal permeability is divided by 3, 60, and 1000, respectively, for modeling cases *B*, *C*, and *D*.

4.1.6 Heat Exchange Simulations of the Stan Sheriff Athletic Complex Site

Where the heating and cooling loads of a GHE system are unbalanced, it is important that heat that is discharged into the subsurface is dissipated through convective heat flow caused by groundwater flow to the sea so that the GHE system retains its efficiency over time. Such a system operates more like a radiator (such as the Verona ground-source heat exchange system, which has over 6,000 ground-source heat exchange boreholes [Hart et al. 2022]), where heat dissipation is needed to maintain the heat balance of the subsurface reservoir over time. Thus, capturing the impact of lateral groundwater flow and its ability to sweep heat out of the system is critical to developing numerical models to help design and predict the system performance. Most GHE models utilize a simple g-function to represent heat exchange between the closed-loop system and the subsurface, which does not capture the thermal impact of lateral groundwater flow, as it only captures the effects of conductive heat transfer. A more rigorous representation of subsurface heat and flow processes can be realized using the TOUGH simulator, which can accurately model the effects of both convective and conductive heat flow. This simulator has been used to model geothermal district heating and cooling systems in stand-alone mode, and has been adapted to connect with the Modelica Buildings Library (Wetter et al. 2014), which includes dynamic simulation models for building and district energy and control systems (e.g., Hu et al. 2021, 2022). However, these coupled studies considered only a single borehole, with a highly resolved grid surrounding it. Here we have 100 boreholes, making this approach impractical for the present early-stage scoping studies of the Stan Sheriff site.

Efforts are underway to make the Modelica/TOUGH coupling practical for large borefields, but in the meantime, here we devise a loosely coupled Modelica/TOUGH interface, as follows. We run Modelica with the g-function to model 1 year of a GHE system with no groundwater flow, incorporating actual load data for the Stan Sheriff Center (see Section 4.2). We then take the resulting loop flow rate (which is constant over time), and inlet temperature to the borefield (which varies hourly) and apply them as a source term for the extra grid blocks representing the boreholes in the TOUGH model. Modelica's loop flow rate is evenly divided between the 100 boreholes, and Modelica's hourly inlet temperatures are averaged to 1-day segments, denoted $T_{in}(t)$ and applied to each borehole. Previous studies have shown that because heat transfer is slow in the subsurface, averaging out daily variability is reasonable, and allows TOUGH to run much more efficiently. Each extra grid block in the TOUGH model also has a sink term with strength equal in magnitude but opposite in sign to the source term. The enthalpy of each sink term is converted to outlet temperature for each borehole, which is then averaged over the 100 boreholes, yielding $T_{out}(t)$. The main outputs of the TOUGH simulations are: (1) the difference between the inlet and outlet temperatures, $DT(t) = T_{in}(t) - T_{out}(t)$, which indicates how effectively the GHE is running, and (2) the spatial distributions of temperature in the subsurface at various times, which illustrate the coupled groundwater and heat flow.

For the present Stan Sheriff load data used, the borehole spacing is sufficiently large so that the subsurface surrounding the boreholes is not heated up enough in 1 year for groundwater sweep of heat to be necessary; TOUGH simulations for the four groundwater flow cases all yield about the same results for DT. This is an interesting finding in itself, but we are really interested in the longer-term behavior of the GHE system. Therefore, we replicate the 1-year Modelica $T_{in}(t)$ data for 10 years and apply that as a source term for a 10-year TOUGH simulation. This replication process is equivalent to assuming that each year the Modelica simulation starts fresh, as would be the case if groundwater flow swept away the heat stored in the previous year.

Figures 19–22 show cross-section and plan views of the subsurface temperature fields after 1, 2, 5, and 10 years of operation, for cases *A* through *D*, respectively. These are simple scatter plots of the temperature of each grid block, making the variable grid resolution apparent. The location of each section is shown by a dashed line in the other section. The red box in the plan view shows the footprint of the 100-borehole borefield. Groundwater flow direction is from A' to A.

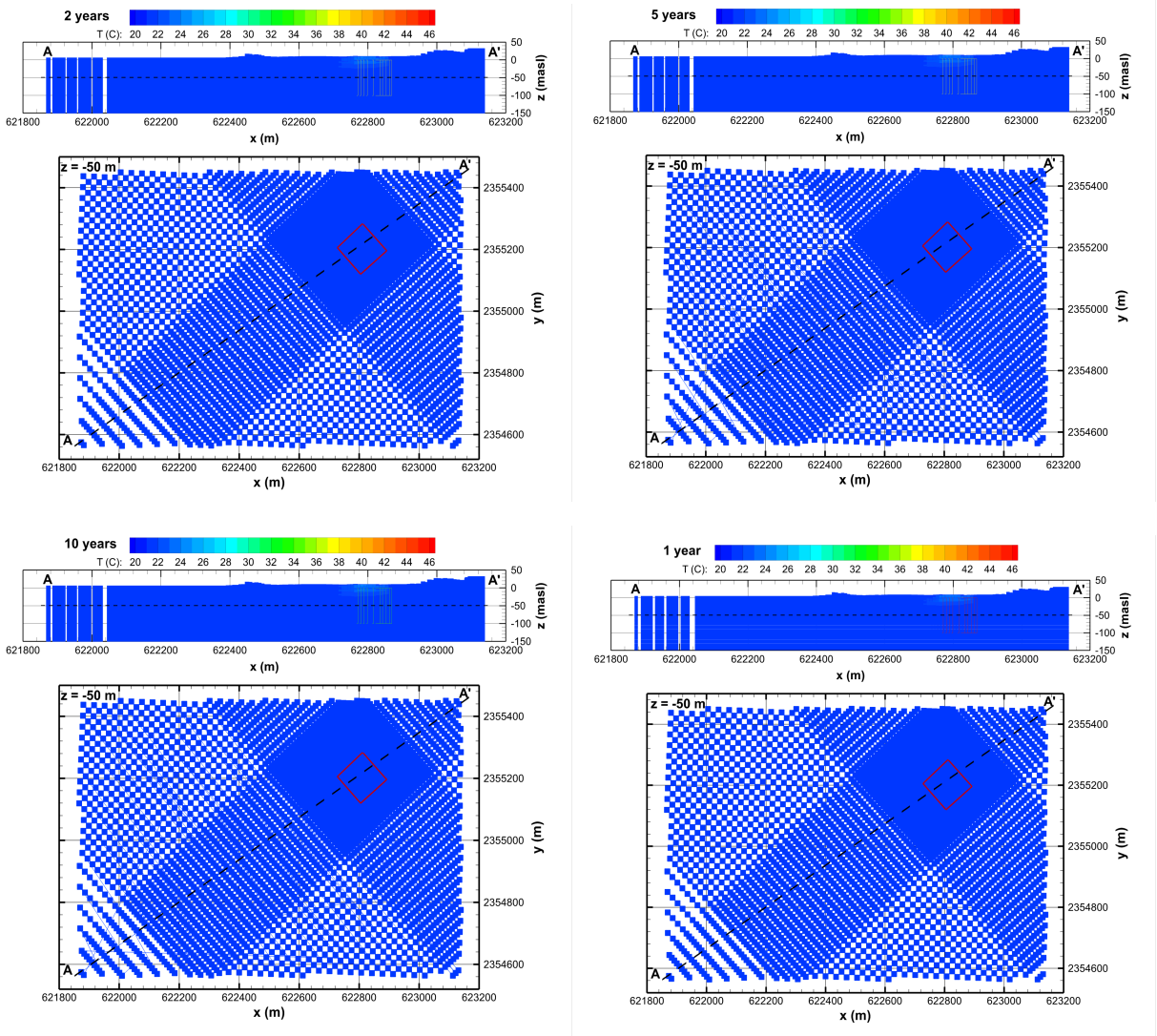

Figure 19. TOUGH simulation results showing vertical cross-section and plan views of the temperature distributions after 1, 2, 5, and 10 years of operation for Case *A*, with extremely large groundwater flow. The red box in the plan view shows the footprint of the 100-borehole borefield. Groundwater flow direction is from A' to A.

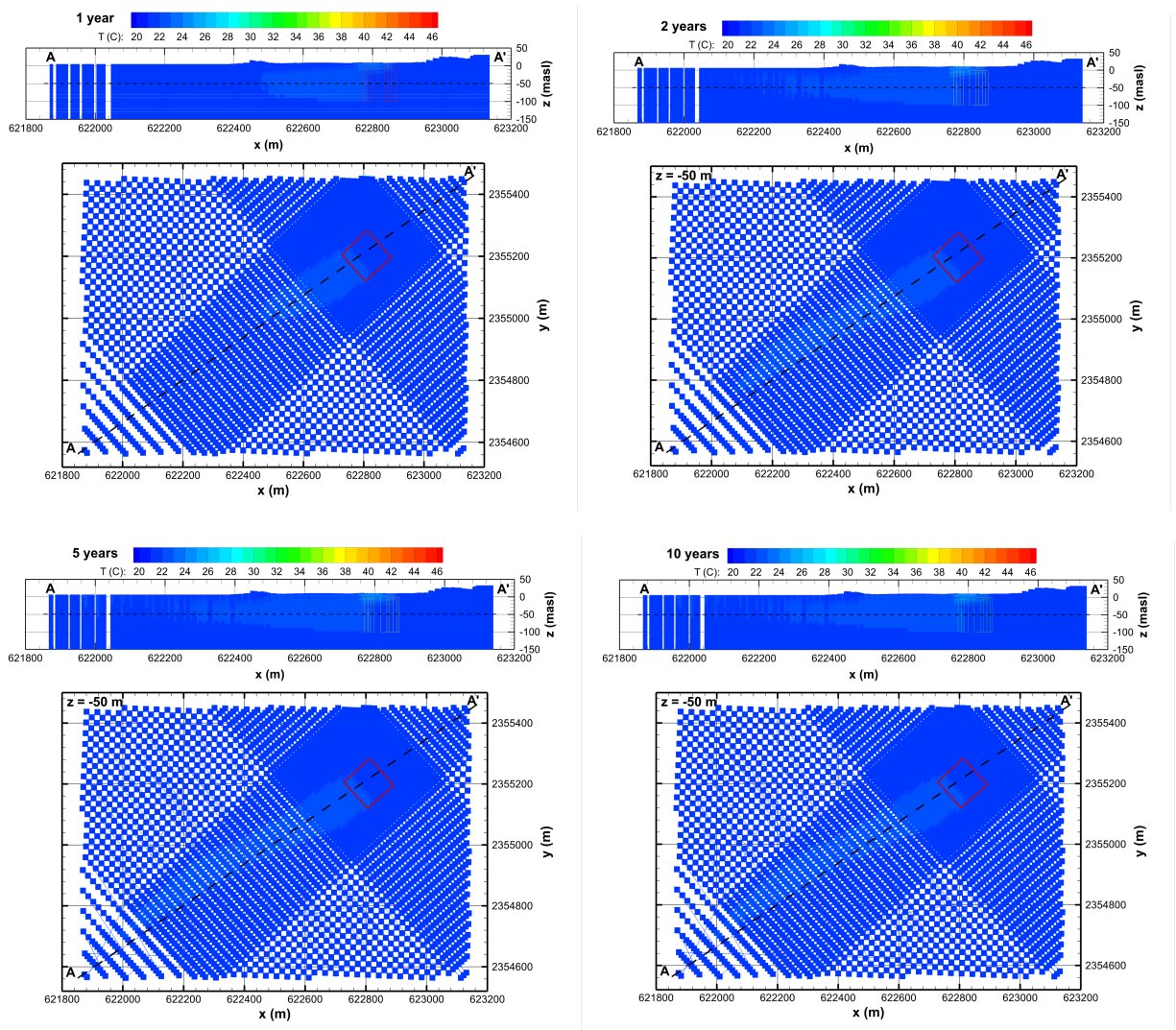

Figure 20. TOUGH simulation results showing vertical cross-section and plan views of the temperature distributions after 1, 2, 5, and 10 years of operation for Case *B*, with large groundwater flow. The red box in the plan view shows the footprint of the 100-borehole borefield. Groundwater flow direction is from A' to A.

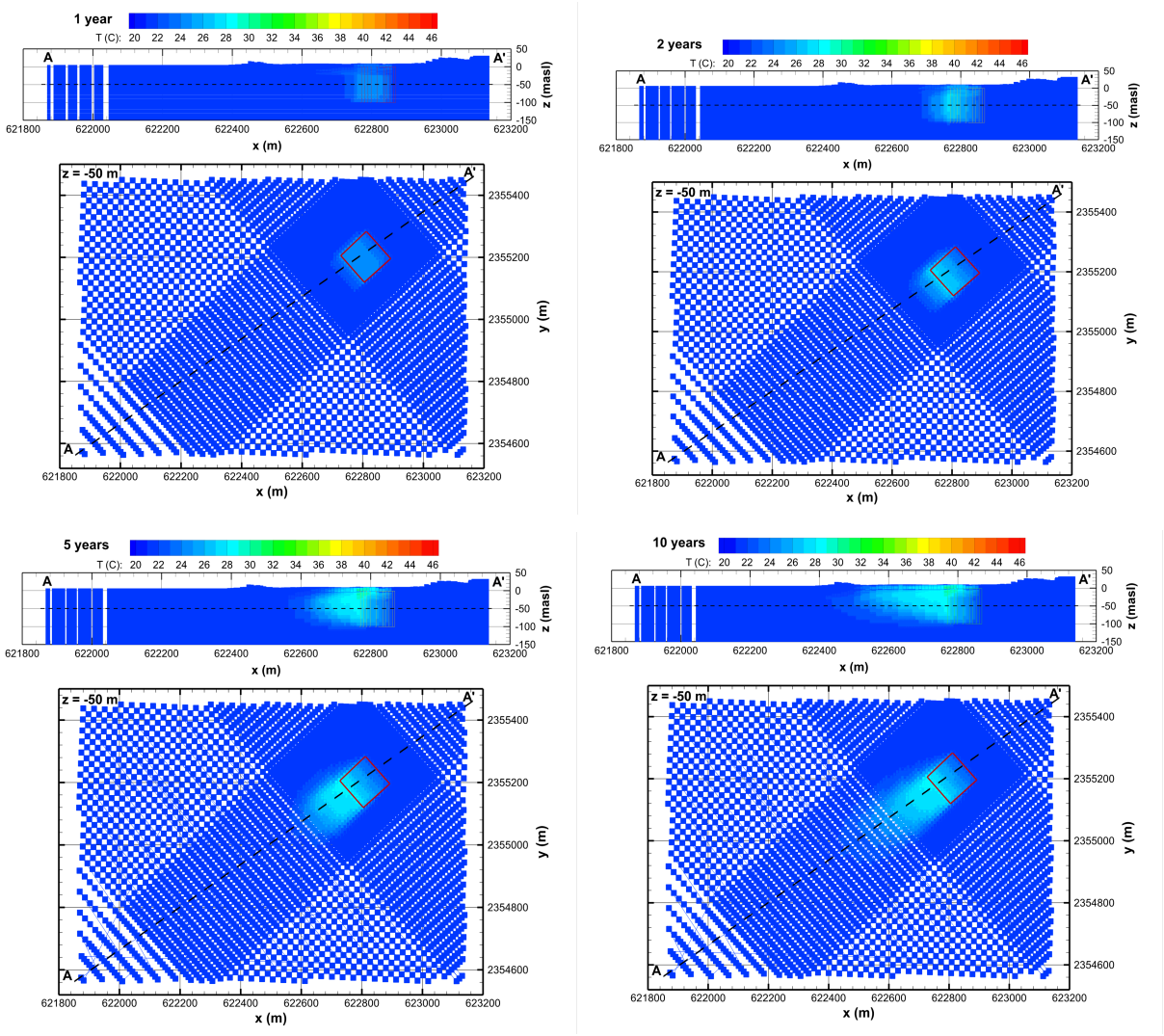

Figure 21. TOUGH simulation results showing vertical cross-section and plan views of the temperature distributions after 1, 2, 5, and 10 years of operation for Case *C*, with moderate groundwater flow. The red box in the plan view shows the footprint of the 100-borehole borefield. Groundwater flow direction is from A' to A.

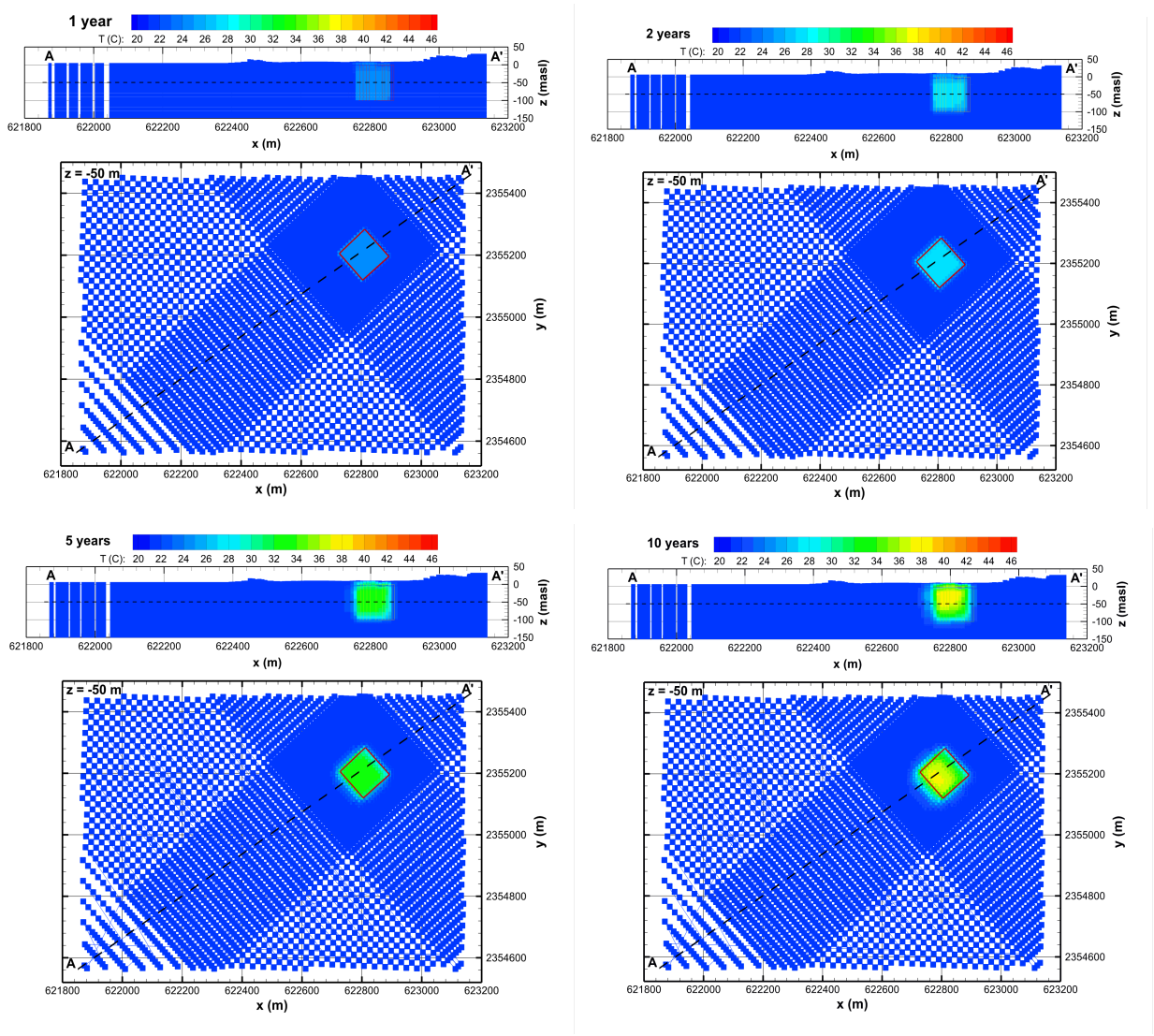

Figure 22. TOUGH simulation results showing vertical cross-section and plan views of the temperature distributions after 1, 2, 5, and 10 years of operation for Case *D*, with minimal groundwater flow. The red box in the plan view shows the footprint of the 100-borehole borefield. Groundwater flow direction is from A' to A.

In Figure 19–Figure 22, the color scale (20–46°C) was chosen to cover the entire range of model temperatures, from initial condition (21.5°C) to inlet temperature (variable from 40 to 52°C, with a mean of 46°C), so the temperature in the borefield can be compared to the inlet temperature. As mentioned above, after 1 year, the borefield temperature is small for all cases, much closer to the initial temperature than to the maximum inlet temperature. So at the start of the second year, the system will behave much as it did during the first year for all cases. In Case *A*, with extremely large groundwater flow, there is almost no temperature increase observed anywhere, because downgradient movement of warmed water is so large that any thermal perturbation is less than the minimum contour level, 1°C. For Case *B*, with large groundwater flow, only a small portion of the borefield itself shows any temperature increase, and the downgradient movement of slightly warmed groundwater is extensive. For Case *C*, with moderate groundwater flow, the borefield temperature is larger than in Case *B*, but it remains small compared to the inlet temperature for all times. Downgradient movement of warmed groundwater is apparent, but it is not as extensive as in case *B*. For Case *D*, with almost no

groundwater flow, a significant temperature increase in the borefield is apparent by two years, and continues to grow thereafter. Downgradient movement of warmed water is minimal. All three cases *A*–*C* show significantly decreased temperature in the borefield compared to Case *D*, indicating that at these magnitudes of groundwater flow, heat sweep away from the borefield is important.

Figure 23–Figure 26 show T_{in}, T_{out}, and DT for Cases *A*–*D*, respectively. Recall that T_{in} is specified from the Modelica simulation, whereas T_{out} and DT are outputs of the TOUGH simulation. At the end of 1 year, DT is about the same for all cases, consistent with the similar 1-year borefield temperatures noted in Figure 19–Figure 22. DT is about the same for Case *A* and Case *B* for all times, and does not change much from year to year, indicating that the large groundwater flow for Case *B* is sufficient to give the GHE a fresh start each year, and the even larger groundwater flow for Case *A* does not add any benefit. For Case *C* with moderate groundwater flow, DT slightly decreases with time beyond 1 year, as the subsurface heats up, and the GHE effectiveness is diminished. The decrease in time of DT is much greater for Case *D* with minimal groundwater flow to sweep heat away, inhibiting the subsurface from accepting more heat.

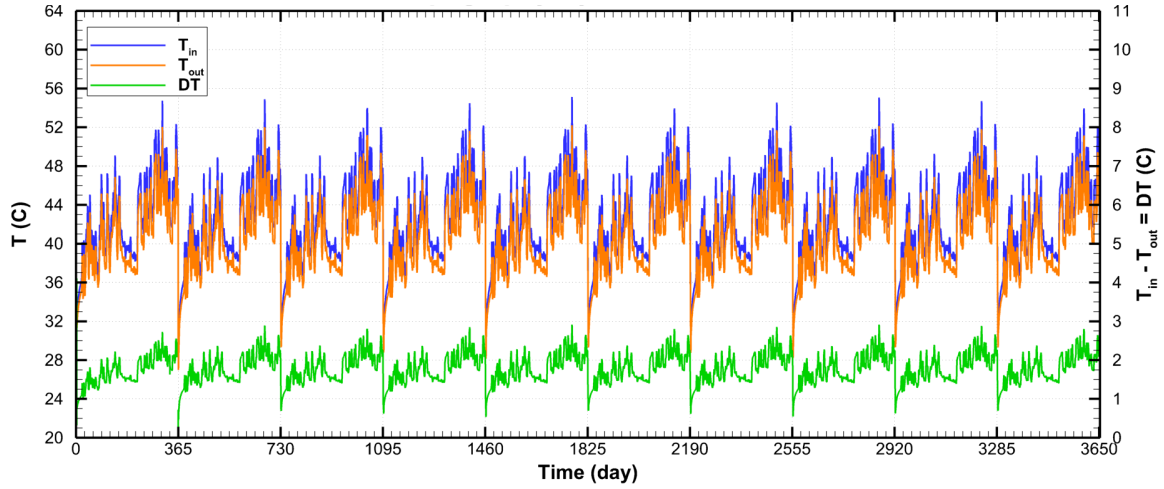

Figure 23. TOUGH simulation results showing T_{in}, T_{out}, and DT for Case *A*, with extremely large groundwater flow

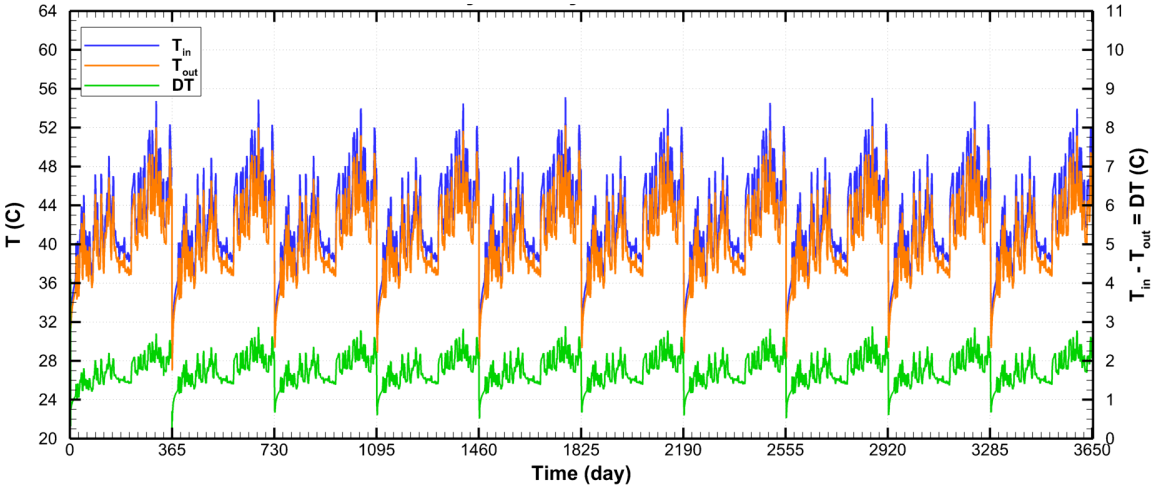

Figure 24. TOUGH simulation results showing T_{in}, T_{out}, and DT for Case *B*, with large groundwater flow

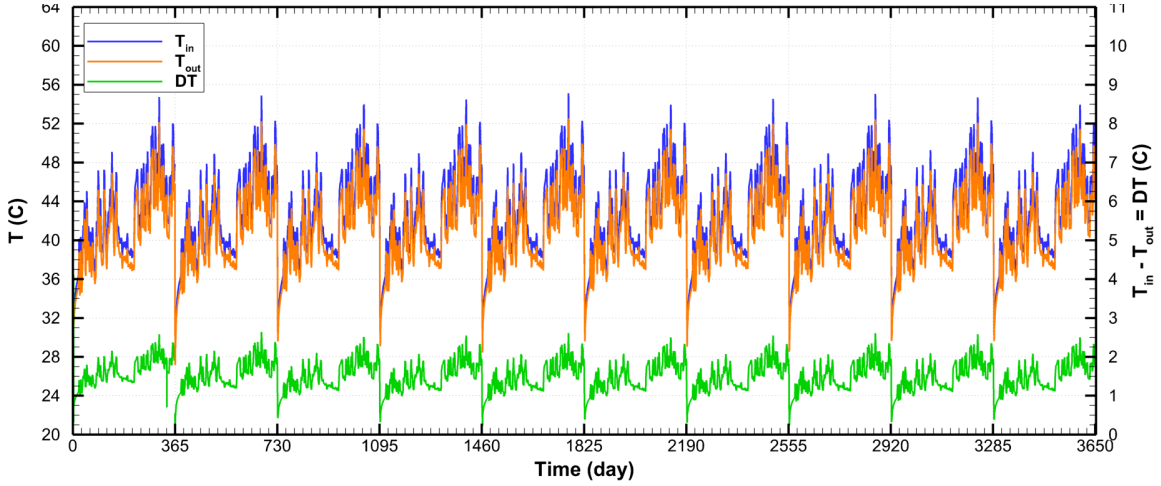

Figure 25. TOUGH simulation results showing T_{in}, T_{out}, and DT for Case *C*, with moderate groundwater flow

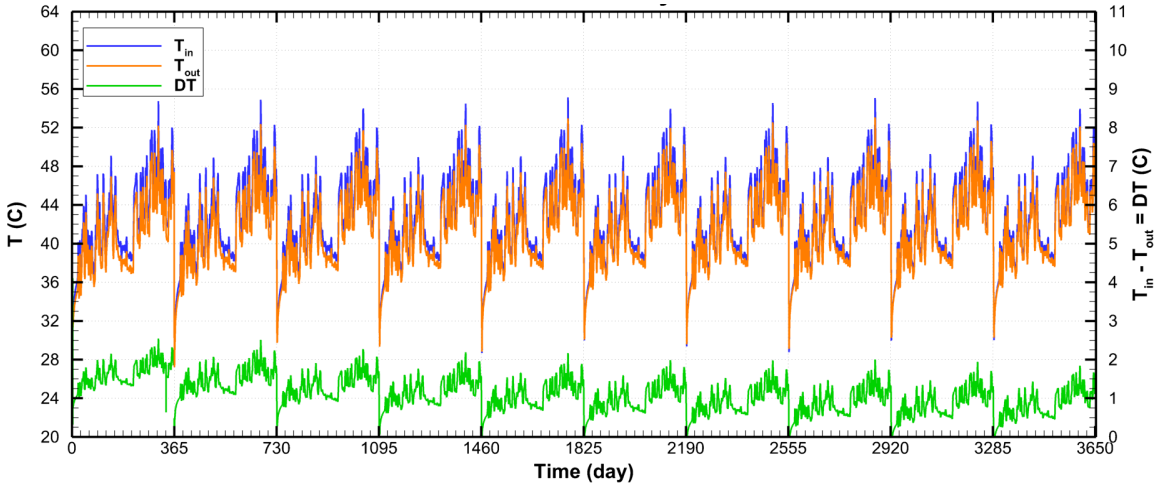

Figure 26. TOUGH simulation results showing T_{in}, T_{out}, and DT for Case *D*, with minimal groundwater flow

4.1.7 Next Steps for Thermo-Hydrogeological Modeling

The TOUGH model can be modified in several ways to improve representation of the hydrogeologic setting. Two simple improvements would be to assign a lower thermal conductivity to represent the drier conditions of the vadose zone, and to assign a more realistic initial temperature profile, as shown in Figure 17, with a larger temperature for the surface boundary condition (Figure 18). More elaborate improvements would be to consider moisture and heat transport in the vadose zone, including precipitation, evaporation, and infiltration of excess irrigation, in order to explain the observed temperature profiles. This would require an Equation of State module including both water and air, which would slow down the simulations considerably. Additionally, a double-porosity or multiple interacting continua method could be used to better represent heat transfer in fractured rock. This would require greatly increasing the number of grid blocks in the model, again slowing down the simulations.

One problem with the more elaborate model improvements described above is that they make an already computationally intensive model even more time-consuming to run. We need to consider these features to

ascertain their impact on heat transfer, but if it is small enough, we may wish to ignore them and continue using a simpler model. Appendix B shows some additional TOUGH simulation results to demonstrate the validity of the current version of the model, and explore additional features.

4.2 Full-GHE-System Modeling With Modelica Building Library

The open-source Modelica Buildings Library (Wetter et al. 2014) developed by Berkeley Lab, which includes dynamic simulation models for building and district energy and control systems, has models for closed-loop borefields (Picard and Helsen 2014), based on so-called g-functions (Claesson and Javed 2012). The models solve the transient heat flux in the ground by discretizing the ground surrounding the borehole in several cylindrical layers. The layer temperature at the outer radius is calculated using an approximation of the line-source theory together with superposition. This model assumes that heat transfer in the ground is purely by conduction, with no ground water flow.

The Modelica model for the Stan Sheriff site includes the actual electrical consumption for the Stan Sheriff Center at 15-minute time intervals, denoted P(t). According to a rule of thumb assumption that HVAC systems typically consume around 70% of a building's base energy usage, with 25%–35% of energy consumed by chillers producing chilled water for air conditioning; we assumed that the chiller consumed 30% of the total energy. The chiller efficiency, which equals the ratio of cooling or heating load to the chiller consumed energy, is assumed to be 4.5. We then converted the actual electrical consumption to the building's cooling load (i.e., $Q_{cool} = (P * 0.3) * 4.5$). We assumed that the water flow from the borefield is the only cooling source for the ground-source heat pump, as shown in Figure 27.

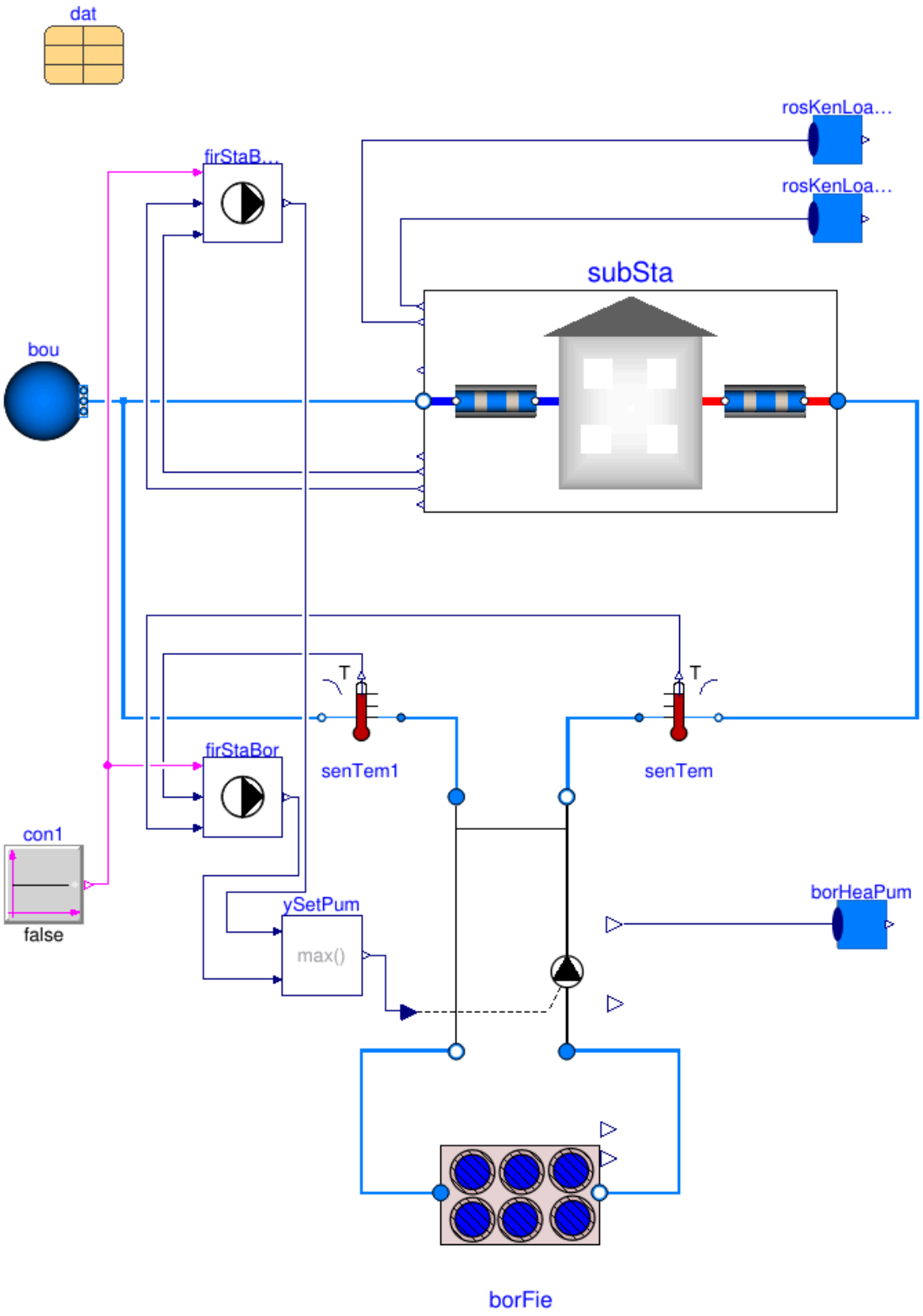

Figure 27. Modelica model for the Stan Sheriff Center with the borefield as the only cooling source. The component "subSta" includes the models for pipes, ground-source heat pump, and building load models.

To understand how different borefield designs and different ground thermal conductivities affect GHE performance, we simulated four cases as described in Table 7 below for a 1-year period. Note that, in these simulations, heat is transferred to the ground by conduction only. Case 1 is the base case. The ground thermal conductivity is doubled in Case 2, and the length of the boreholes is increased from 100 m to 150 m in Case 3; both changes are designed to increase the heat transfer between the boreholes and the ground. We halved the number of boreholes in Case 4, to see whether a smaller (and thus cheaper to construct) GHE would be viable.

Table 7. Modelica Simulation Cases

Case	Soil Conductivity (W/m/K)	Borehole Length (m)	Number of Boreholes
1	2	100	100
2	4	100	100
3	2	150	100
4	2	100	50

The results shown in Figure 28 indicate that, with the doubled soil conductivity (Case 2), the water temperatures in and out of the borefield are lowest and the heat pump consumes the least amount of power. For longer boreholes (Case 3), water temperatures and heat pump power consumption are lower than for the base case, but not as low as for Case 2. In contrast, for Case 4 with half the number of boreholes, the water becomes much hotter and the heat pump power requirements are correspondingly much greater.

Figure 29 shows the results for the entire 1-year simulation for Cases 1 and 2, including water temperatures and cumulative heat pump energy consumption, which is the time-integral of the heat pump power shown in Figure 28. For both cases, water temperatures show a gradual increase. For Case 1, the entire year heat pump energy consumption is 2.92e6 MJ, while for Case 2, the consumption is 1.88e6 MJ, which is reduced by 55% from Case 1. This indicates that with enhanced heat transfer from the boreholes to the ground, such as would occur if significant ground water flow swept accumulated heat away, the system performance would be significantly improved.

Figure 29 shows results of a 10-year simulation of Case 2, the best-performing of the four cases. The increase in water temperatures, which was modest after 1 year (Figure 29), is quite large by 10 years, implying that the heat pump power requirements would be too large to make operation of the GHE viable, for any of the scenarios with no groundwater flow.

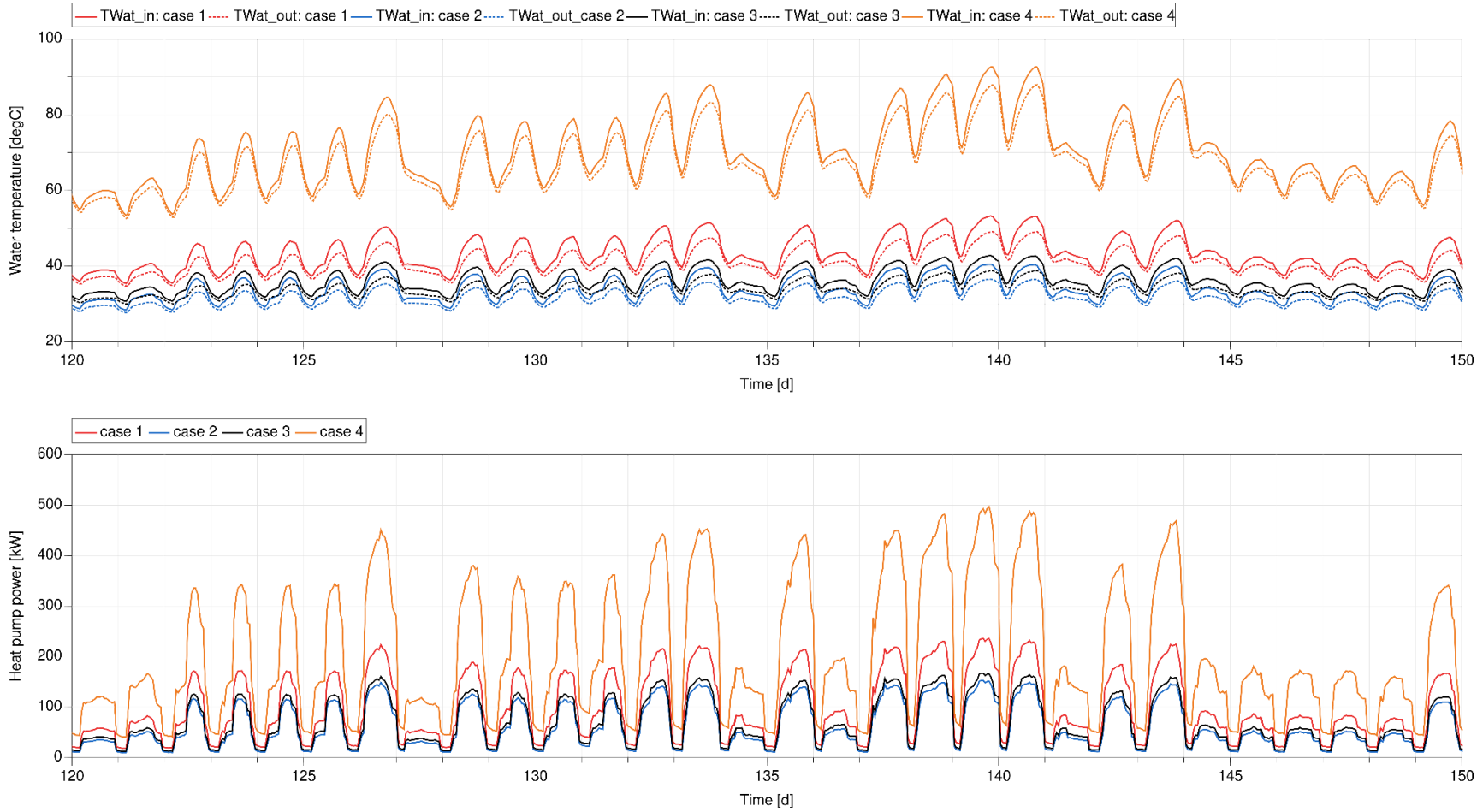

Figure 28. Modelica simulation results (from Day 120 to Day 150) for the 1-year simulation of all four cases. Top: water temperature in and out of the borefield; bottom: heat pump power consumed.

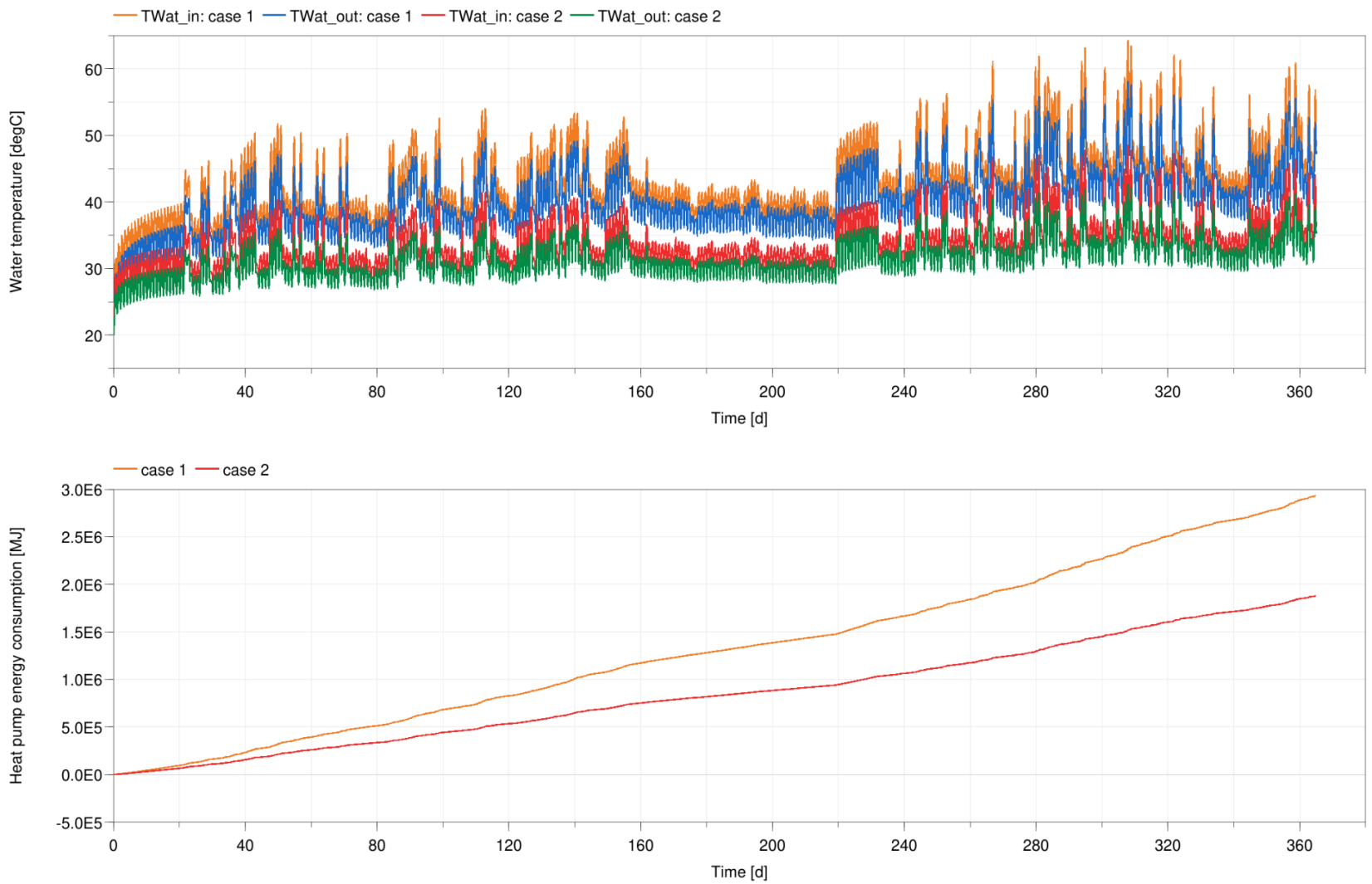

Figure 29. Results of the 1-year Modelica simulations of Cases 1 and 2. Top: water temperature in and out of the borefield; bottom: integrated heat pump energy consumption. The difference between the end points of each profile shows the entire year's energy consumption.

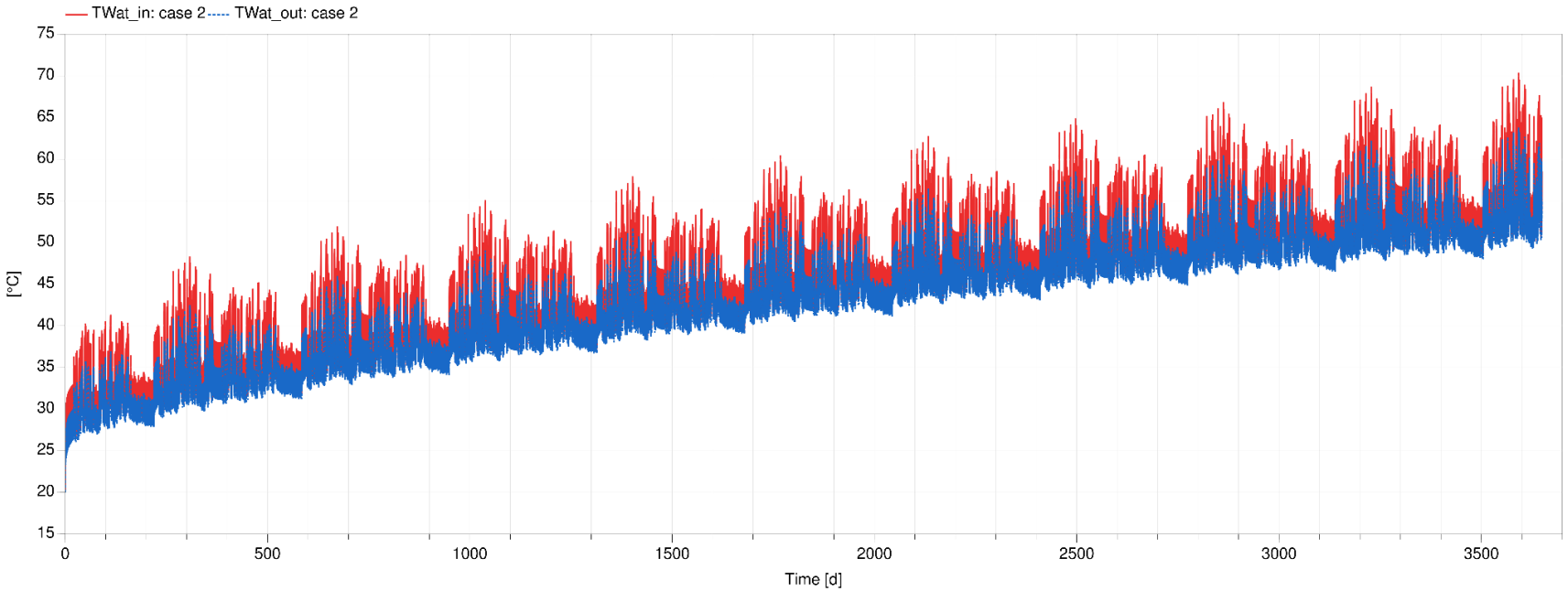

Figure 30. Water temperature in and out borefield for 10-year Modelica simulation of Case 2.

4.3 Economic Analysis

4.3.1 Data and Methods

UH provided interval metering data for the Stan Sheriff building for January 21, 2022, through December 31, 2022. So that we could calculate bill impacts over a full year, we assumed that the hourly load profile for January 1–20 was the same as the hourly average of the load between January 21–31. This approach assured that the diurnal pattern of the imputed electricity usage reflects Hawai‘i’s climate in January. We recognize that building occupancy in the first two weeks of January may be less than that during the second half of the month due to the university’s holiday schedule. Our estimate of electricity usage for the two weeks of January, therefore, may be slightly biased upwards. The overall impact of this bias on our results is likely small because it only affects 2 weeks of the year.

We estimated the net present value (NPV) of the geothermal exchange system, accounting for electricity bill savings, the cost of the geothermal system, tax credits introduced by the Inflation Reduction Act, and a range of loan terms. We assume that the chiller remains in the building and that the geothermal system does not avoid future chiller replacements.

4.3.1.1 Electricity Bill Savings

We determined electricity bill savings by multiplying annual electricity and monthly peak demand reductions and by the energy ($/kWh) and demand ($/monthly kW) components of UH’s electricity tariff. We calculated hourly electricity savings by subtracting post-geothermal simulated chiller demand from pre-geothermal chiller demand. We estimated pre-geothermal chiller demand from the metered building-level demand by assuming that the chiller accounted for 30% of the building’s energy demand in all hours. The first three Modelica models of the geothermal system and its interactions with the building’s HVAC system described in Section 4.2 provided 1-year estimates of simulated post-geothermal chiller demand.

Importantly, the Modelica models do not account for the impact of subsurface water flow. However, they only cover 1 year, too short a time for a significant amount of heat to build up in the subsurface. We assume that the post-geothermal load profile repeats annually for the 20-year lifetime of the geothermal system. By concatenating the 1-year demand profiles from the Modelica simulations, we represent conditions in which subsurface water flow prevents a buildup of heat. We validate this assumption by analyzing a 10-year simulation of Modelica Models 1 and 2, which results in net increases in building power demand after 2 and 6 years, respectively. The net increase in demand indicates that the geothermal system is not viable when there is no groundwater flow to remove the built-up heat. Due to the lack of access to campus-wide metering data, we were not able to estimate the reduction in chiller demand that was coincident with the campus-wide peak demand, which Hawaiian Electric uses to determine the University’s demand charge. Instead, we estimated the minimum likely reduction in coincident peak demand attributable to the geothermal exchange system’s impacts on chiller electricity consumption. For each hour of the day in each month, we identified the maximum reduction in chiller demand (e.g., the maximum chiller demand reduction at 4 p.m. in June). For each month, we then took the minimum reduction during the hours in which peak demand could reasonably occur (12–8 p.m.). This process resulted in a conservative estimate of the peak demand reduction from the geothermal exchange system in each month of the year. We multiplied each of these demand reductions by the $27.85 per kW demand charge to determine monthly demand charge savings.

4.3.1.2 System Costs

We then estimated the cost of the system by multiplying the geothermal system size (in tons) by $10,000 per ton, a cost provided to us by an industry expert. Costs may be higher for Hawai‘i, given its remote location. We set the system size to meet peak chiller demand, which we assumed aligned with peak power flow through

the borefield in the Modelica simulations. The Modelica simulations provided the water temperature entering into and exiting from the borefield and the flow rate of the water (in kg/s). The flow was a constant 64.5 kg/s in all hours of the simulation. We estimated the peak power in the borefield in tons by taking the average of the 20 highest absolute changes in temperature across the borefield, and multiplying it by the specific heat of water (4186 J/kg*C), flow rate, and unit conversions for watts per ton. Table 8 summarizes the temperature changes and peak borefield power for Simulations 1–3.

Table 8. Temperature Deltas and Peak Borefield Power in Modelica Simulations

Simulation	Average of 20 Highest Absolute Temperature Changes (℃)	Peak Borefield Power (tons)
1	5.9	451
2	5.5	424
3	5.7	428

4.3.1.3 Tax Credits and Loan Terms

We calculated NPV for three tax credit levels and two types of credits established in the Inflation Reduction Act for geothermal systems, direct pay and transfer, relative to the case of no tax credit. The first tax credit level of 6% is the base credit for eligible systems. The second level of 30% applies to geothermal systems less than 1 MW or to projects that meet prevailing wage and apprenticeship requirements. The third tax credit level is 40%, which has the same conditions as the second level in addition to domestic content requirements for the geothermal system. With direct pay, eligible entities, including universities, receive tax credit from the IRS in the tax year that they place the equipment into service. We modeled direct pay in the NPV calculation by adding the tax credit to the first year of the discounted cashflows. With transfer credits, eligible entities, including universities, can designate a third party to claim the credit. As a state university, UH is eligible for both credit types. We modeled transfer credits in the NPV calculation by reducing the loan principal by the tax credit amount.

For each chiller simulation, tax credit level, and tax credit type, we calculated NPV for a range of loan repayment periods (10, 15, and 20 years) and interest rates (0%, 2.5%, 5%, 7.5%, 10%, 12.5%) to account for uncertainty in the loan terms that UH would face.

4.3.2 Techno-Economic Analysis Results

Across the first three geothermal system configurations simulated in Modelica, we estimate that annual building-level electricity usage falls by 14%–20% and chiller usage falls by 46%–73%. These electricity reductions equate to annual electricity bill savings of $151,000–$223,000, or 16%–26% of the pre-project building-level annual electricity costs. Energy savings account for 83%–84% of the overall bill savings, with demand charge savings accounting for the remainder of the savings.

We limit the presentation of NPV results to the scenarios that include the highest electricity-saving Modelica simulation (Simulation 2). The estimated geothermal system cost for this system was $4.24 million, which corresponds to a system size of 424 tons. This approach sets an upper bound on the expected financial performance of the project given our input assumptions and methods.

We find that the NPV of the geothermal exchange system increases with longer loan terms, lower interest rates, and higher tax credit levels. For a 10-year repayment period, we did not find a positive NPV for any combination of interest rates and tax credits. For a 15-year loan term, NPV was positive with a 30% or 40% tax credit (claimed or transferred) at zero interest or 40% tax credit (claimed or transferred) at 2.5% interest. As shown in Figure 31 and Figure 32, we estimate positive NPVs for a broader combination of tax credits and interest rates with a repayment period of 20 years for claimed and transferred credits, respectively. NPVs range from about $400,000 with no tax credit and zero interest rates to $2.2 million with a 40% tax credit and zero interest rate. The project can also have positive NPVs at higher interest rates with a 20-year loan term if paired with the highest tax credit level: At 5% interest rate and a 40% tax credit, we estimate an NPV of about $280,000 and $370,000 for claimed and transferred credits, respectively.

Reductions in system costs, additional incentives, or higher electricity prices would increase NPVs and potentially make projects viable at shorter repayment periods and higher interest rates. Internal revolving loan funds could provide low interest rates that make positive project NPV more likely.

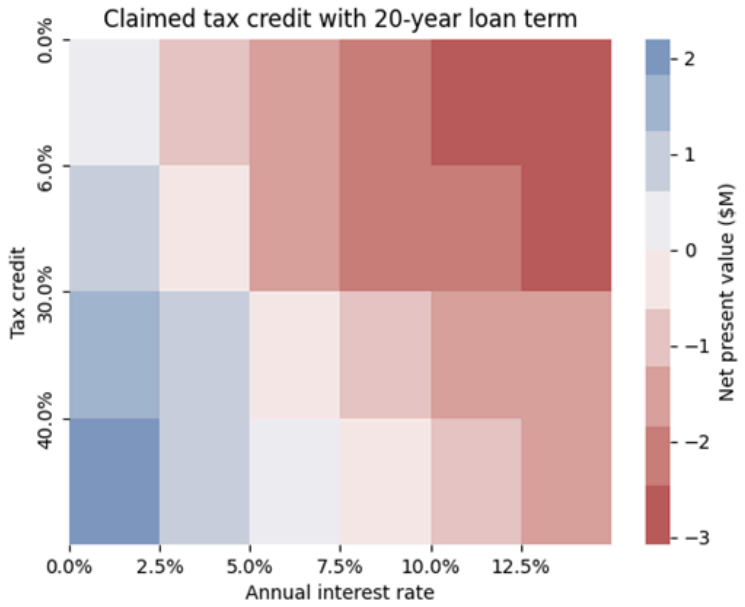

Figure 31. NPV for claimed tax credit with 20-year loan term by tax credit and interest rate

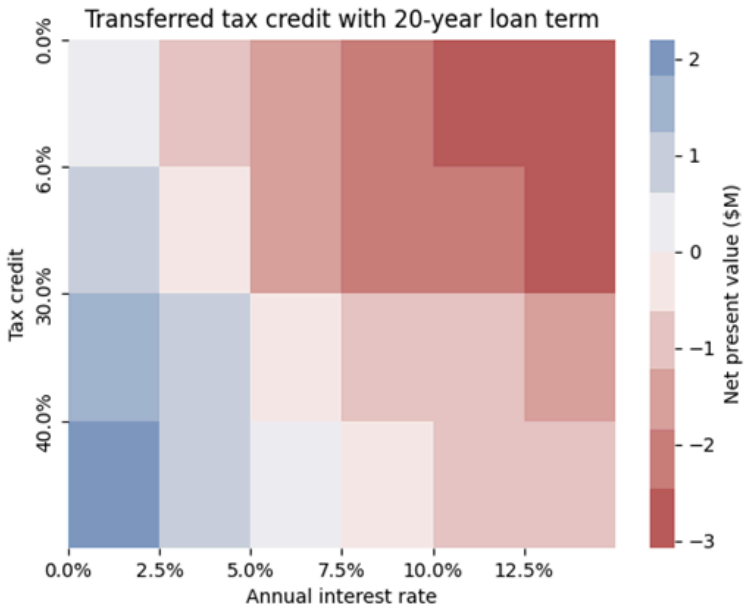

Figure 32. NPV for transferred tax credit with 20-year loan term by tax credit and interest rate

Figure 33 shows the impact on NPV from transferring tax credits instead of claiming them. We find higher NPVs from cases with transferred tax credits, except for when the interest rate is zero, in which case there is no difference. As interest rates increase, the benefit of transferring tax credits increases as well due to the reduced principal and loan payments. We recognize that, in practice, transfer credits may carry transaction costs that mean the principal is reduced by less than the tax credit. However, the potential for higher NPV suggests that UH may benefit from transferring tax credits as opposed to claiming them.

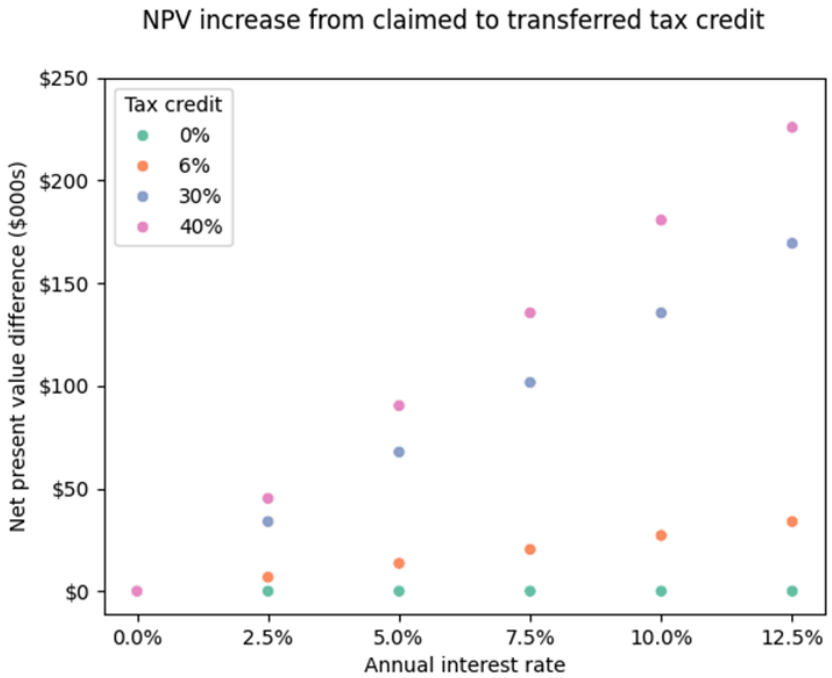

Figure 33. Increase in NPV from transferring relative to claiming tax credit

5. Discussion and Conclusions

We have investigated the feasibility of developing a GHE for Hawai‘i at two scales, the regional (island wide) scale and the site-specific scale. For the Hawaiian climate, the load is cooling-dominated, so there will be a buildup of subsurface heat over time, which must be removed for the continued effective use of the GHE. Hawai‘i’s geography (mountainous terrain) and geology (fractured lava and basalt) favor strong groundwater flow, which we investigated as a means to sweep heat away from the GHE.

At the whole-island scale, a GIS approach is used to develop overall favorability maps for closed-loop and open-loop systems for O‘ahu. The favorability maps sum up rankings for 11 physical and regulatory parameters. Only one parameter differs between the two types of systems, with open-loop systems being precluded from regions where groundwater must be left in its natural state. Overall favorability maps for both closed-loop and open-loop systems show several highly favorable locations, in coastal areas of Ewa, Maili, Haleiwa, Kahuku, Kaneohe, and Honolulu. The highlands of the Ko‘olau and Wai‘anae ranges have generally lower favorability for closed-loop systems, and are largely precluded for open-loop systems.

At a specific site, the Stan Sheriff Athletic Complex at the UH Manoa campus, we have used three methods to assess feasibility of a GHE to meet cooling load: (1) numerical modeling with TOUGH of coupled subsurface heat transport and groundwater flow, loosely coupled to Modelica to provide heat source/sink information; (2) numerical modeling of the full GHE system with Modelica, with subsurface heat flow assumed to be by conduction only (no groundwater flow); and (3) techno-economic analysis.

TOUGH modeling shows the evolution of the thermal plume arising from the cooling-dominated load for the Stan Sheriff Center, for various groundwater flow strengths. For groundwater flow magnitude expected to be representative of the Stan Sheriff Center, heat is effectively swept away from the borefield, enabling the GHE to operate successfully for at least 10 years.

In contrast, Modelica modeling of the no-groundwater flow case shows that although it may operate successfully for 1 year, shortly thereafter the buildup of heat begins to increase water temperatures significantly. Economic analysis indicates that there will be a net increase in chiller demand within 2–6 years, depending on model parameters chosen, rendering the GHE not viable. When groundwater flow is included in an approximate way, by replicating the 1-year Modelica results for 10 years, the economic analysis of the most optimistic case (Model 2 with 100 100-m long boreholes, double thermal conductivity) indicates that the system can yield net benefits to UH if the university is able to utilize tax credits from the Inflation Reduction Act and access low-interest and long-term capital.

The fact that obtaining net benefits from the closed-loop GHE relies on favorable financing and tax credits confirms that the fundamental temperature regime, with groundwater temperature so close to air temperature, makes constructing a viable GHE challenging. The same conclusion would arise for an open-loop system using groundwater. Therefore, despite the technical challenges, we want to continue considering cooler seawater source systems (e.g., Leraand and Van Ryzin 1995). A pilot seawater cooling system has been operating for several decades at the Natural Energy Laboratory of Hawai‘i, along the western coast of the island of Hawai‘i (Daniel 1989). The right location can provide relatively easy access to cold water, which will enable much bigger temperature differences than shallow groundwater systems, and thus result in better GHE performance.

The present loose coupling between Modelica and TOUGH for the situation with strong groundwater flow and many boreholes provides useful insights into coupled groundwater and heat flow and can serve as the basis for preliminary economic analyses. But using the fully coupled Modelica/TOUGH capability, heretofore only used for single boreholes, is much preferred, and will be the subject of follow-on studies.

Acknowledgments

This project was supported by the U.S. Department of Energy's Energy Technology Innovation Partnership Project with the University of Hawai'i (UH) and under the U.S. Department of Energy Award Number DE-AC02-05CH11231 with Lawrence Berkeley National Laboratory. We thank our colleagues Miles Topping and Kendal Leonard at UH, Mark Glick (formerly with UH, now at the Hawai'i State Energy Office) and Dora Nakafuji (formerly of Kamehameha Schools) for their contributions to this project. In particular, Miles Topping provided the load data for the Stan Sheriff Center that was invaluable to the project. The geologic model output for this paper was generated using Leapfrog Software, copyright Seequent Limited. Leapfrog and all other Seequent Limited product or service names are registered trademark or trademarks of Seequent Limited. We thank Jay Egg for sharing his insights with our team on deploying geothermal heat pumps in tropical environments. We also thank Nancy Matsumoto from the Honolulu Board of Water Supply for generously sharing measured thermal profiles from three deep monitoring wells near the Stan Sheriff study area.

References

Claesson, J. and Javed, S. A load-aggregation method to calculate extraction temperatures of borehole heat exchangers. *ASHRAE Transactions* 118(1), (2012), 530–539. https://buildingphysics.com/download/local_163661.pdf

Clague, D.A., Frey, F.A., Garcia, M.O., Huang, S., McWilliams, M., and Beeson, M.H. "Compositional heterogeneity of the Sugarloaf melilite nephelinite flow, Honolulu Volcanics, Hawai'i." *Geochimica et Cosmochimica Acta* 185, (2016), 251–277. https://www.sciencedirect.com/science/article/pii/S0016703716300217

Clark, S.P., Jr. (ed.) *Handbook of Physical Constants – Revised Edition.* Geological Society of America, Memoir 97, (1966). https://pubs.geoscienceworld.org/gsa/books/edited-volume/101/Handbook-of-Physical-Constants

Daniel, T.H. "New seawater delivery systems at the Natural Energy Laboratory of Hawaii." Proceedings Eleventh Annual ASME Solar Energy Conference, (1989), 19 p. https://www.researchgate.net/publication/305490767_New_Seawater_Delivery_Systems_at_the_Natural_Energy_Laboratory_of_Hawaii

Dores, D., and Lautze, N. "Preliminary assessment of ground-source heat exchangers for cooling in Hawai'i." *Sustainable Energy Technologies and Assessments* 37, (2020), 100579. https://www.sciencedirect.com/science/article/abs/pii/S2213138819305971

Doughty, C., Lautze, N., Dobson, P. Ulrich, C, Hu, J., Murphy, S, Thomas, D., and Campton M. "Shallow geothermal resources for cooling applications at the University of Hawai'i." *GRC Transactions* 48, (2024). https://www.geothermal-library.org/index.php?mode=pubs&action=view&record=1035091

Hu, J., Doughty, C., Dobson, P., Nico, P., and Wetter, M. "Coupling subsurface and above-surface models for optimizing the design of borefields and district heating and cooling systems in the presence of varying water-table depth." Proceedings, 46th Workshop on Geothermal Reservoir Engineering, Stanford University, Stanford, CA, (2021). https://pangea.stanford.edu/ERE/db/IGAstandard/record_detail.php?id=29563

Falta, R., L. Murdoch, C. Hammock, K. Bicknell, J. McDaniel, J. Horvath. "Simulation of high temperature subsurface thermal energy storage using closed-loop borehole heat exchangers." TOUGH Symposium 2023, Berkeley, CA, September 18-20, (2023). https://docs.google.com/presentation/d/1yMLigkS9_NesC1wGPtXSFczUmodeVyBb/edit#slide=id.p13

Finstick, S.A. *Subsurface geology and hydrogeology of downtown Honolulu with engineering and environmental implications.* Ph.D. Thesis, Department of Geology and Geophysics, UH Manoa, (1996). https://scholarspace.manoa.hawaii.edu/items/ff333640-26f2-4a30-bc82-a7c6ac727d49

Halliday, W.R. "History and status of the Moiliili Karst, Hawaii." *Journal of Cave and Karst Studies* 60(3) (1998), 141–145. https://www.caves.org/wp-content/uploads/Publications/JCKS/v60/V60N3-Halliday.pdf

Hart, D.J., Tinjum, J.M., Fratta, D., Thomas, L.K., and Carew, E.L. "Radiators or reservoirs: Heat budgets in district-scale ground-source geothermal exchange fields." Proceedings, 47th Workshop on Geothermal Reservoir Engineering, Stanford University, (2022). https://pangea.stanford.edu/ERE/db/IGAstandard/record_detail.php?id=35400

Hu, J., Doughty, C., Dobson, P., Nico, P., and Wetter, M. "Coupling subsurface and above-surface models for optimizing the design of borefields and district heating and cooling systems in the presence of moving groundwater." Proceedings, 47th Workshop on Geothermal Reservoir Engineering, Stanford University, (2022). https://pangea.stanford.edu/ERE/db/IGAstandard/record_detail.php?id=35405

Hunt, C.D., Jr. *Geohydrology of the Island of Oahu, Hawaii*. U.S. Geological Survey Professional Paper 1412-B, (1996). https://pubs.usgs.gov/publication/pp1412B

Izuka, S.K., Engott, J.A., Rotzoll, K., Bassiouni, M., Johnson, A.G., Miller, L.D., and Mair, A. *Volcanic aquifers of Hawai'i – Hydrogeology, water budgets, and conceptual models.* U.S. Geological Survey Scientific Investigations Report 2015-5164, version 2.0, (2018). https://pubs.usgs.gov/publication/sir20155164

Izuka, S.K., and Rotzoll, K. *Volcanic aquifers of Hawai'i – Contributions to assessing groundwater availability on Kaua'i, O'ahu, and Maui*. U.S. Geological Survey Professional Paper 1876, (2023). https://pubs.usgs.gov/publication/pp1876

Jung, Y., G.S.H. Pau, S. Finsterle. C. Doughty. *TOUGH3 User's Guide, Version 1.0*, Rep. LBNL-2001093, Lawrence Berkeley Laboratory, Berkeley, Calif., (2018). https://escholarship.org/uc/item/0dh2w4w6

Lau, L.S., and Mink, J.F. *Hydrology of the Hawaiian Islands*. University of Hawaii Press, (2006). https://www.jstor.org/stable/j.ctt6wr37p

Leraand, T.K., and Van Ryzin, J.C. "Air conditioning with deep seawater: A cost-effective alternative for West Beach, Oahu, Hawaii." Proceedings of the IEEE Oceans 1995 Conference, (1995), 1100–1109. https://ieeexplore.ieee.org/document/528579

Liu, C.C.K. *RAM2 modeling and the determination of sustainable yield of Hawai'i basal aquifers*. Water Resources Research Center Project Report PR-2008-06; (2007), 81 p. https://files.hawaii.gov/dlnr/cwrm/publishedreports/PR200806.pdf

Liu, X., Ho, J., Winick, J., Porse, S., Lian, J., Wang, X., Liu, W., Malhotra, M., Li, Y., and Anand, J. *Grid cost and total emissions reductions through mass deployment of geothermal heat pumps for building heating and cooling electrification in the United States.* Oak Ridge National Laboratory Report ORNL/TM-2023/2966, (2023). https://www.osti.gov/biblio/2224191

Nichols, W.D., Shade, P.J., and Hunt, C.D., Jr. *Summary of the Oahu, Hawaii, regional aquifer-system analysis*. U.S. Geological Survey Professional Paper 1412-A, (1996). https://pubs.usgs.gov/publication/pp1412A

Milicich, S.D., Alcaraz, S., and Pearson-Grant, S.C. "An integrated approach to geological and fluid flow modelling: From a 3D geological model to TOUGH2." Proceedings, 37th New Zealand Geothermal Workshop, 18–20 November 2015, Taupo, New Zealand, (2015). https://worldgeothermal.org/geothermal-data/conference-paper-database

Oki, D.S., *Geohydrology of the central Oahu, Hawaii, ground-water flow system and numerical simulation of the effects of additional pumping*, U.S. Geological Survey, Water-Resources Investigations Report 97-4276, (1998). https://pubs.usgs.gov/publication/wri974276

Okuhata, B. *Development of a model to identify local hydrogeology and simulate groundwater injection in Nuuanu and Kalihi aquifer systems, Oahu, Hawaii*. Masters Report, Department of Geology and Geophysics, UH Manoa, (2017). https://www.soest.hawaii.edu/GG/academics/theses/Okuhata_MS_Final_Report.pdf

Picard, D. and Helsen L. "Advanced Hybrid Model for Borefield Heat Exchanger Performance Evaluation: an Implementation in Modelica." Proceedings, the 10th International Modelica Conference, p. 857–866. Lund, Sweden. March 2014. https://2014.international.conference.modelica.org/proceedings/html/submissions/ECP14096857_PicardHelsen.pdf

Pruess, K. *Brief guide to the MINC-method for modeling flow and transport in fractured media*. Lawrence Berkeley National Laboratory Report LBL-32195, (1992). https://escholarship.org/uc/item/38r1c71c.

Robertson, E.C. *Thermal properties of rocks*. U.S. Geological Survey Open-File Report 88-441, (1988). https://pubs.usgs.gov/of/1988/0441/report.pdf

Rotzoll, K., and El-Kadi, A.I. "Estimating hydraulic conductivity from specific capacity for Hawaii aquifers, USA." *Hydrogeology Journal* 16, (2008), 969-979. researchgate.net/profile/Aly-El-Kadi/publication/225548816_Estimating_hydraulic_conductivity_from_specific_capacity_for_Hawaii_aquifers_USA/links/55efd02c08ae0af8ee1b3d59/Estimating-hydraulic-conductivity-from-specific-capacity-for-Hawaii-aquifers-USA.pdf

Rotzoll, K., Oki, D.S., and El-Kadi, A. "Changes in freshwater-lens thickness in basaltic island aquifers overlain by thick coastal sediments." *Hydrogeology Journal* 18, (2010), 1425-1436. https://www.researchgate.net/publication/225132691_Changes_of_freshwater-lens_thickness_in_basaltic_island_aquifers_overlain_by_thick_coastal_sediments

Sherrod, D.R., Sinton, J.M., Watkins, S.E., and Brunt, K.M. "Geologic map of the State of Hawaii." U.S. Geological Survey Scientific Investigations Map SIM-3143, (2021). https://pubs.usgs.gov/publication/sim3143

Wetter, M., Zuo, W., Nouidui, T.S., and Pang, X.: Modelica Buildings library, *J. Building Performance Simulation* 7, (2014) 253–270. https://www.tandfonline.com/doi/epdf/10.1080/19401493.2013.765506

Wolf, J.E. *Map location and dimensional definition of subsurface caverns*. Senior Thesis, Department of Geology and Geophysics, University of Hawai'i, (1975). https://scholarspace.manoa.hawaii.edu/items/fe2c02a9-bae9-4dc0-8441-18e0435deb5c

Appendix A. Parameters Used for GIS Favorability Maps

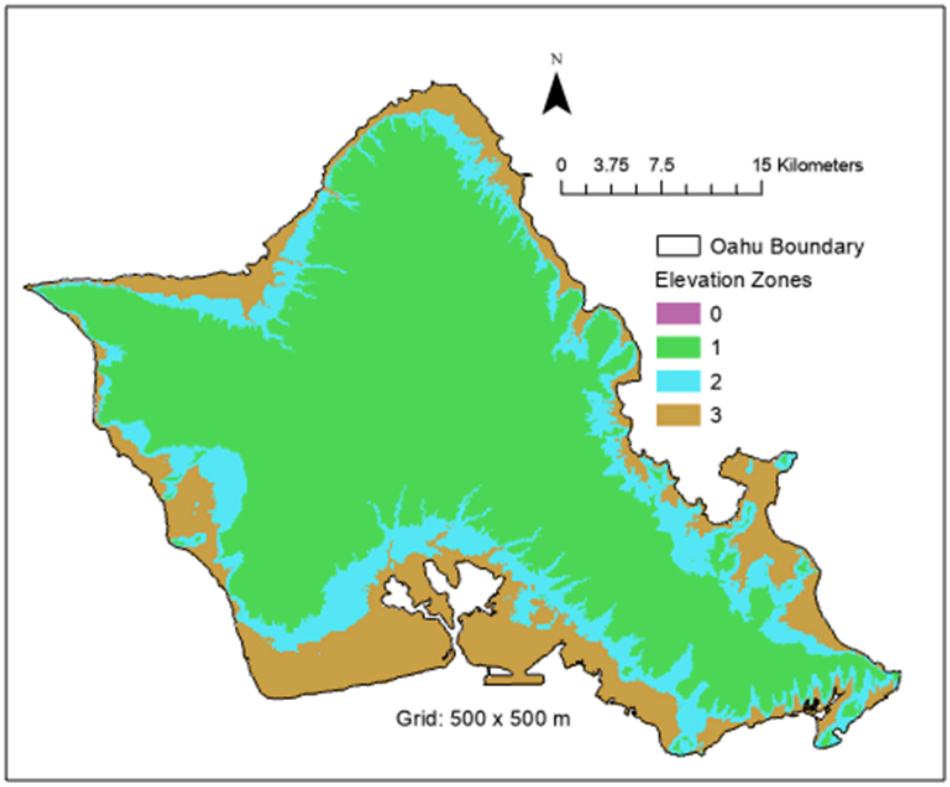

s

Figure A- 1. Elevation favorability map

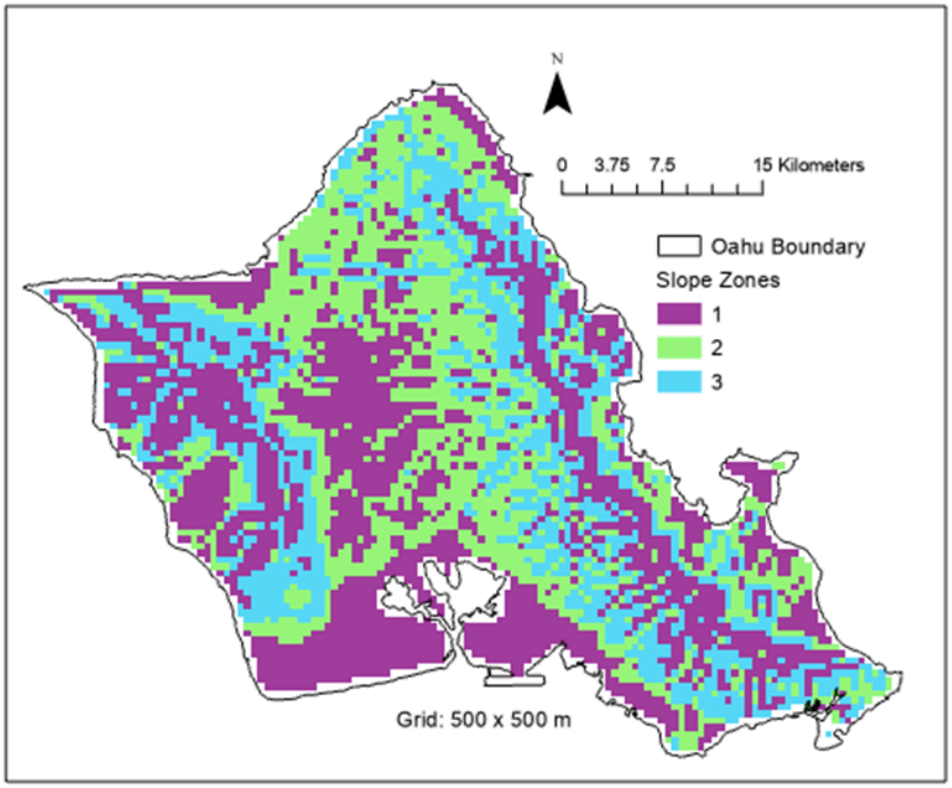

Figure A- 2. Slope favorability map

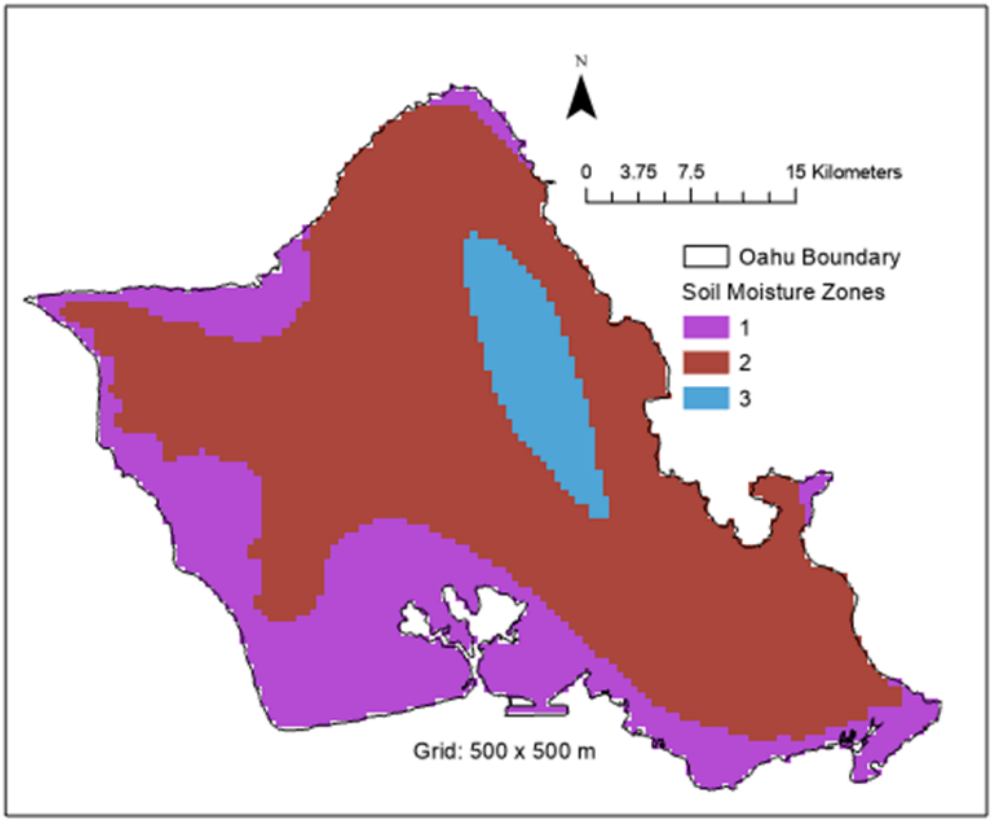

Figure A- 3. Soil moisture favorability map

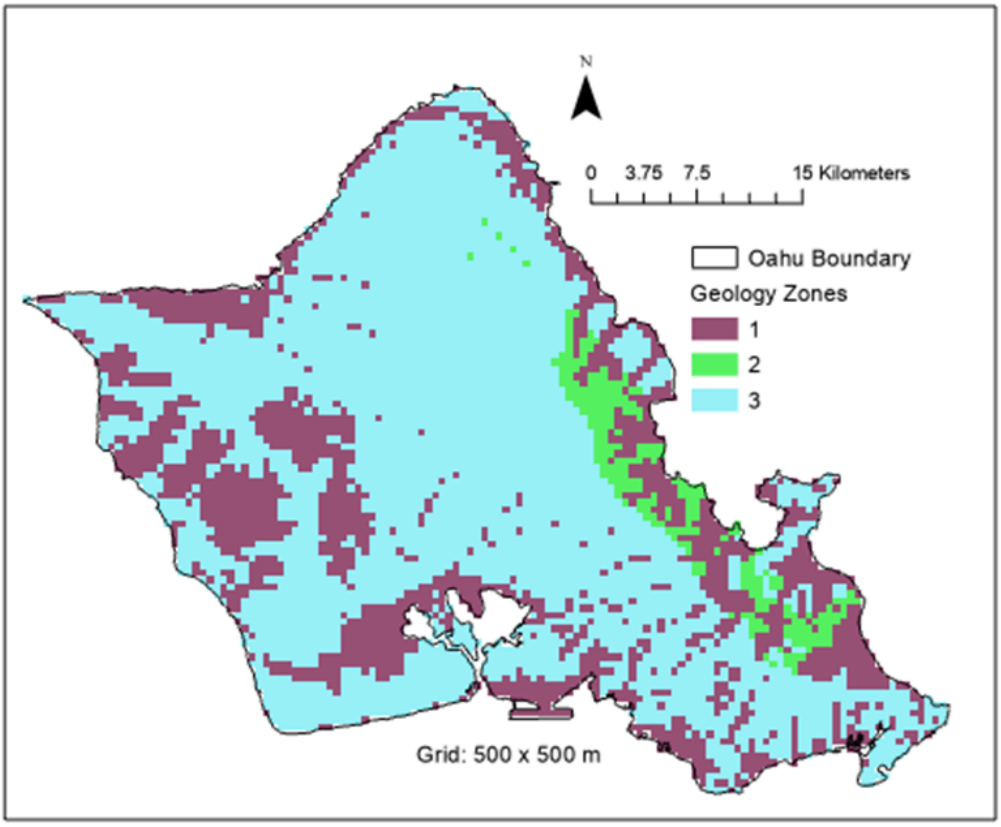

Figure A- 4. Geology favorability map

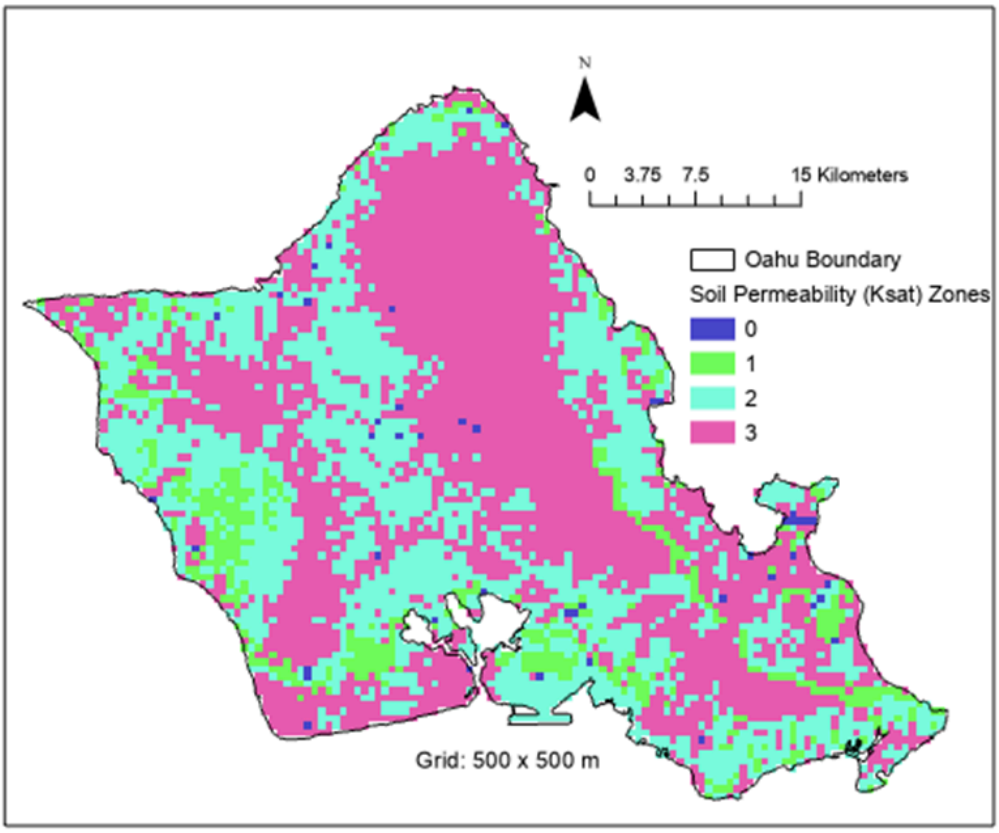

Figure A- 5. Soil permeability (Ksat) favorability map. Ksat depicts how fast water can drain through the material: 0) not available; 1) slow < 0.3 m/day; 2) moderate 0.3–1 m/day; 3) fast 1–10 m/day or very fast > 10 m/day

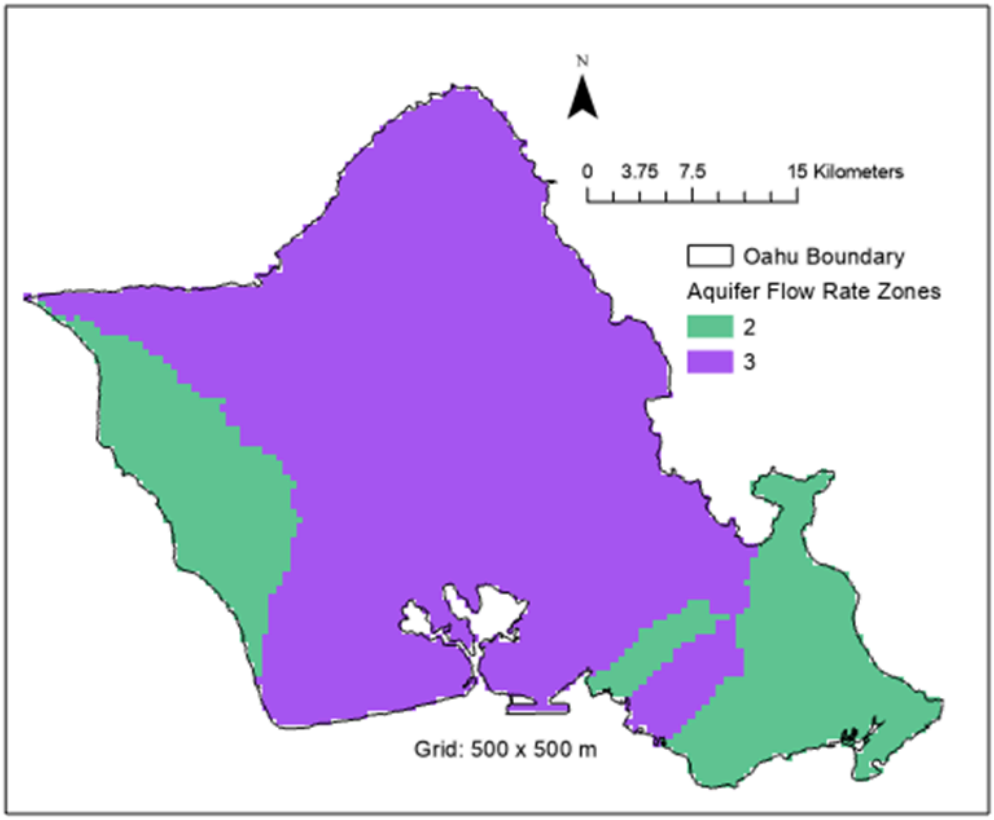

Figure A- 6. Aquifer flow rate favorability map

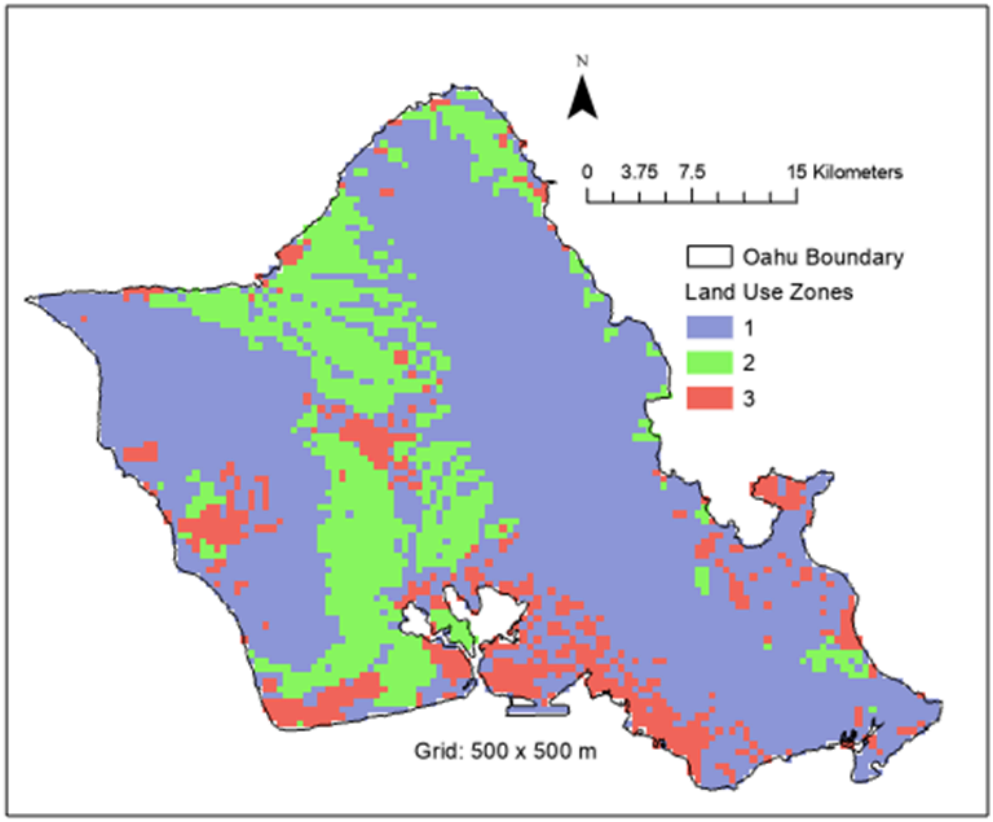

Figure A- 7. Land use favorability map

Table A- 1. Land Cover Favorability

Land Use/land Cover	Favorable 12, 13, 16, 17	Somewhat Favorable 22, 24	Unfavorable 11, 14, 31, 32, 33, 42, 53, 54, 61, 62, 75, 76

Table A- 2. Land Cover Codes

Main Category	Individual Category Code	Main Category	Individual Category Code
1. Urban or built-up land	11. Residential	4. Forest Land	41. Deciduous Forest Land
	12. Commercial and Services		42. Evergreen Forest Land
	13. Industrial		43. Mixed Forest Land
	14. Transportation, Communications, and Utilities	5. Water	51. Streams and Canals
	15. Industrial and Commercial Complexes		Lakes
	16. Mixed Urban or Built-up Land		Reservoirs
	17. Other Urban or Built-up Land		Bays and Estuaries
2. Agricultural Land	21. Cropland and Pasture	6. Wetland	61. Forested Wetland
	22. Orchards, Groves, Vineyards, Nurseries and Ornamental Horticultural Areas		62. Nonforested Wetland
	23. Confined Feeding Operations	7. Barren Land	71. Dry Salt Flats
	24. Other Agricultural Land		72. Beaches
3. Rangeland	31. Herbaceous Rangeland		73. Sandy Areas Other than Beaches
	32. Shrub and Brush Rangeland		74. Bare Exposed Rock
	33. Mixed Rangeland		75. Strip Mines, Quarries, and Gravel Pits
			76. Transitional Areas
			77. Mixed Barren Land

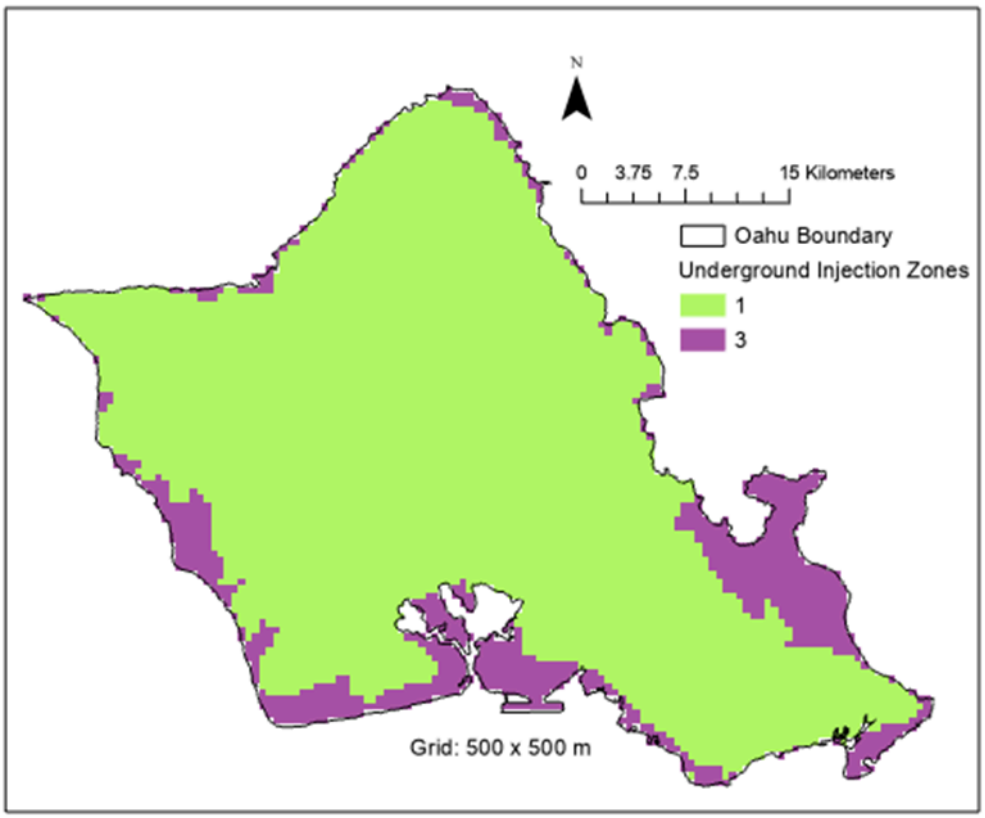

Figure A- 8. Underground injection favorability map

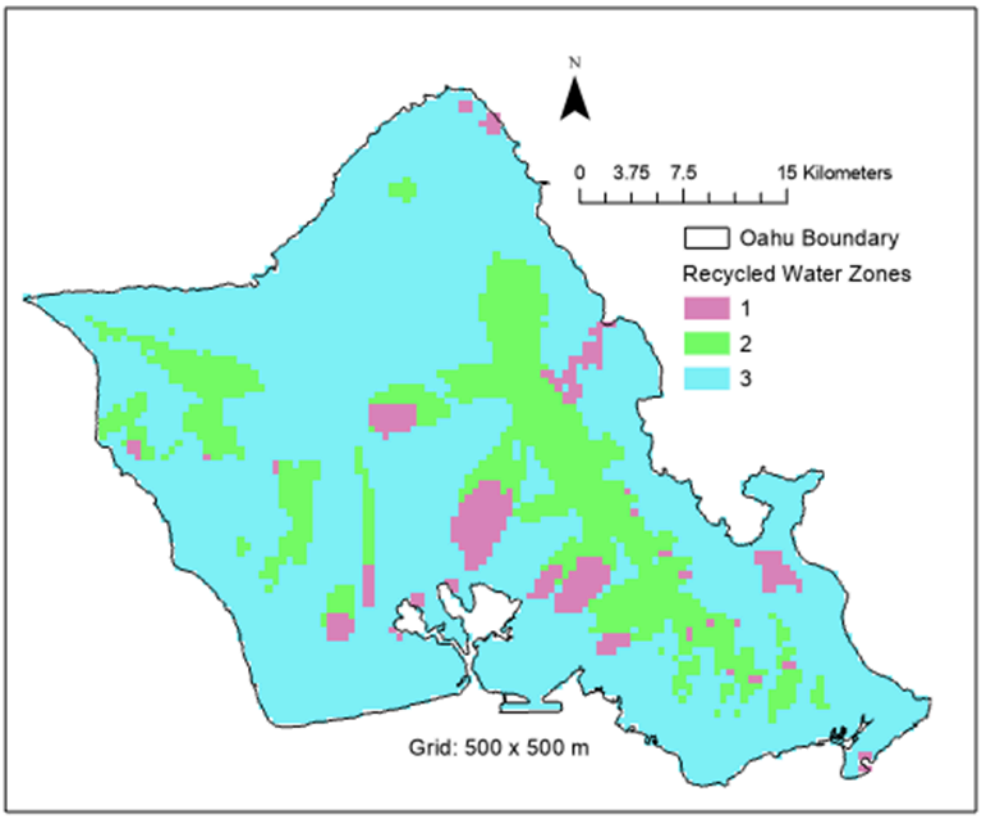

Figure A- 9. Recycled water favorability map

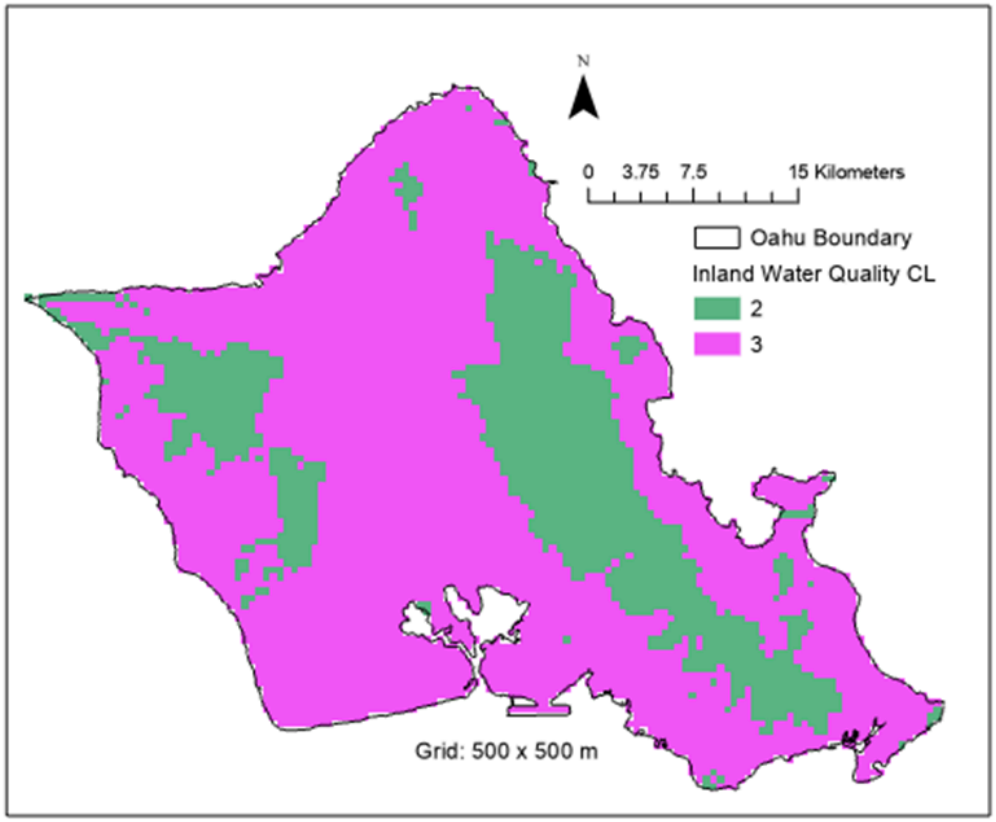

Figure A- 10. Inland water quality (closed loop) favorability map

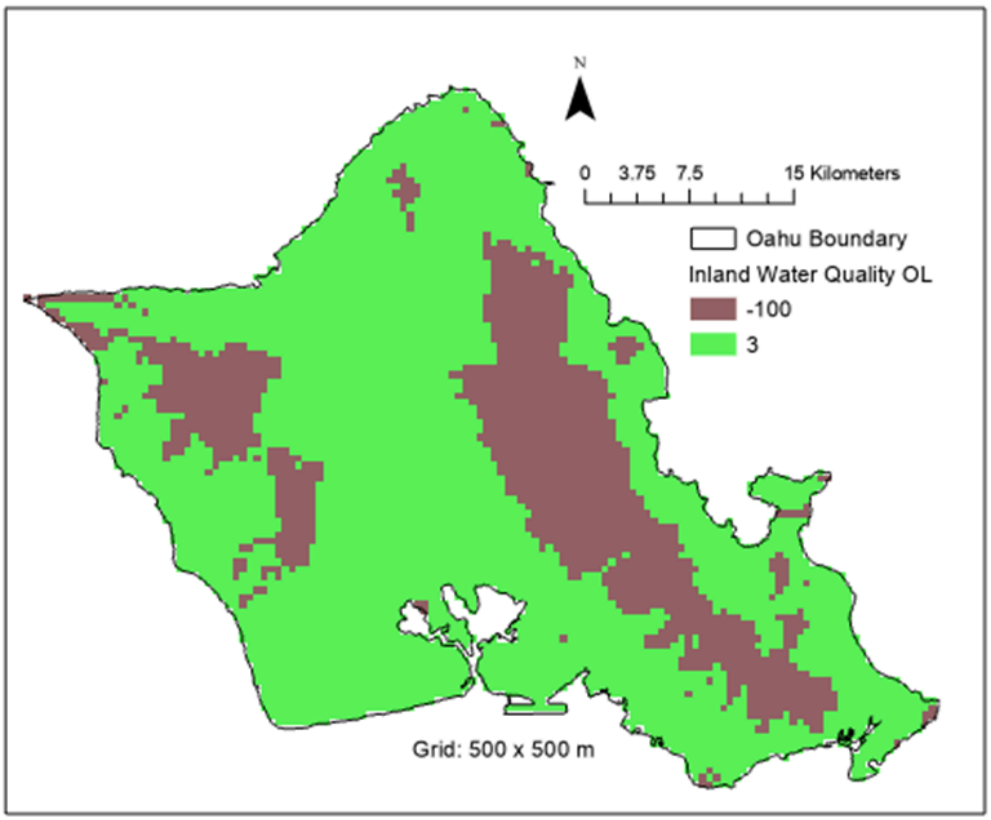

Figure A- 11. Inland water quality (open loop) favorability map

Appendix B. Additional TOUGH Simulation Results

B.1 Verification of Extra Grid Block Method to Represent Boreholes

The "extra grid block" method to represent boreholes, described in Section 4.1.3, enables TOUGH to represent hundreds of individual boreholes within a borefield in a very efficient way. To verify that this method produces accurate results, we compare Modelica and TOUGH results for a 10-year Modelica simulation of Case 1, the base case. The TOUGH model uses Case *D*, which uses base-case properties but decreased permeability to produce minimal groundwater flow, to be comparable to the Modelica g-function, which assumes heat transfer occurs by conduction only. The TOUGH simulation takes T_{in}, the inlet temperature to the borefield, provided at 1-hour intervals by Modelica, and averages it into 1-day intervals to use as source terms for all the boreholes. The TOUGH simulation then produces T_{out}, the average outlet temperature from all the boreholes, at 1-day intervals. Figure B- 1 shows T_{in}, which is the same for Modelica and TOUGH, T_{out} from Modelica, and T_{out} from TOUGH, for three 1-year time periods at the beginning, middle, and end of the 10-year simulation. The TOUGH T_{out} values match the Modelica T_{out} values well overall, but are a bit high early and a bit low late.

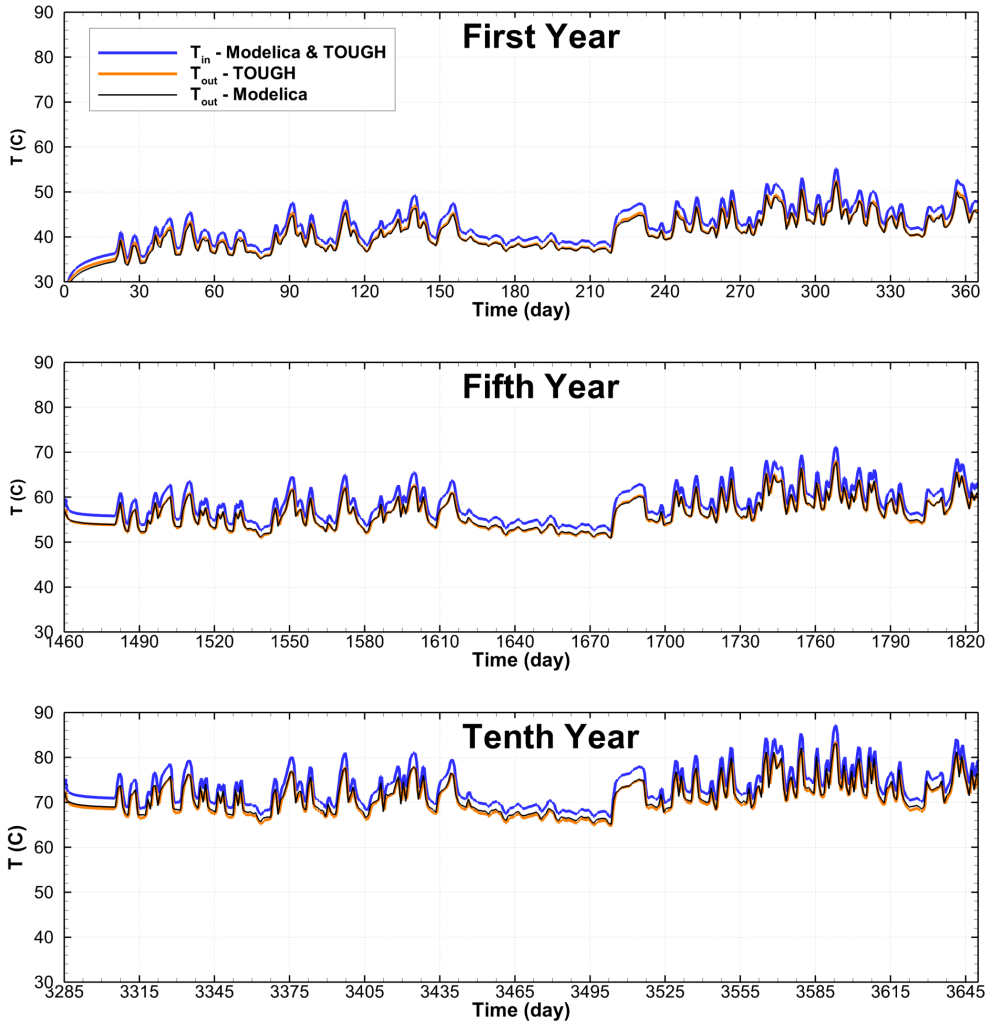

Figure B- 1. Verification of extra grid block method to represent boreholes. T_{in} and T_{out} for a 10-year simulation of Modelica Case 1 (base case) and TOUGH Case *D* (base case, except minimal groundwater flow).

B.2 Verification of Time-Averaging of Modelica Inlet Temperature

The Stan Sheriff load data is provided at 15-minute intervals, and is time-averaged within Modelica to provide T_{in} at 1-hour intervals. Because temperature changes occur slowly within the subsurface, T_{in} is averaged to 1-day intervals before being provided as source terms to TOUGH. Significantly, this averaging removes diurnal temperature variations, but enables TOUGH to take 1-day time steps as opposed to 1-hour time steps, significantly reducing required computation time. To verify that this averaging does not produce systematic errors in the TOUGH simulation results, a 1-year simulation of Case *D* was done using 4-hour averaging of T_{in} and compared to the 1-day averaged results, as shown in Figure B- 2. Using 4-hour averaging enables diurnal variations to be represented, while still providing a reasonable usage of computer time. The agreement between Modelica and TOUGH T_{out} values for the 4-hour averaging is comparable to that for the 1-day averaging overall, but, interestingly, the agreement is better at night (minimum daily temperature). The relationship between the 4-hour averaged results and the 1-day average results is as expected, with diurnal variations being smoothed out in a reasonable way. More importantly, the spatial temperature distributions for the two TOUGH simulations (not shown) are indistinguishable.

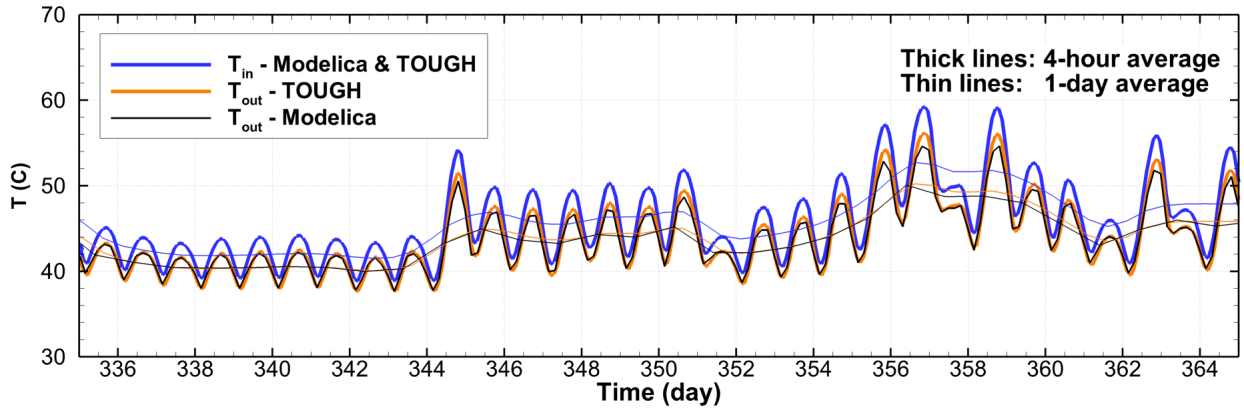

Figure B- 2. Verification of time-averaging of inlet temperature. T_{in} and T_{out} for the final month of 1-year simulations of Modelica Case 1 (base case) and TOUGH Case *D* (base case, except minimal groundwater flow), using either 4-hour averaging (thick lines) or 1-day averaging (thin lines).

B.3 Using Variable Initial Temperature Profile in TOUGH Simulation

A 10-year simulation of a variation on Case *D* was done, using the March 14, 2024, temperature profile from Kaimuki Pump Station (Figure 17) as the initial temperature condition in the model instead of a uniform value of 21.5°C. The temperature at the ground surface (27°C) from the temperature profile was used as the constant-temperature surface boundary condition for the model. Using these conditions has no discernible effect on the operation of the GHE for the minimal groundwater flow case (i.e., $T_{out}(t)$ is unchanged from Figure 23). The spatial temperature distribution (Figure B- 3) illustrates that the differences in the temperature distributions shallow and deep are minor compared to the temperature in the borefield.

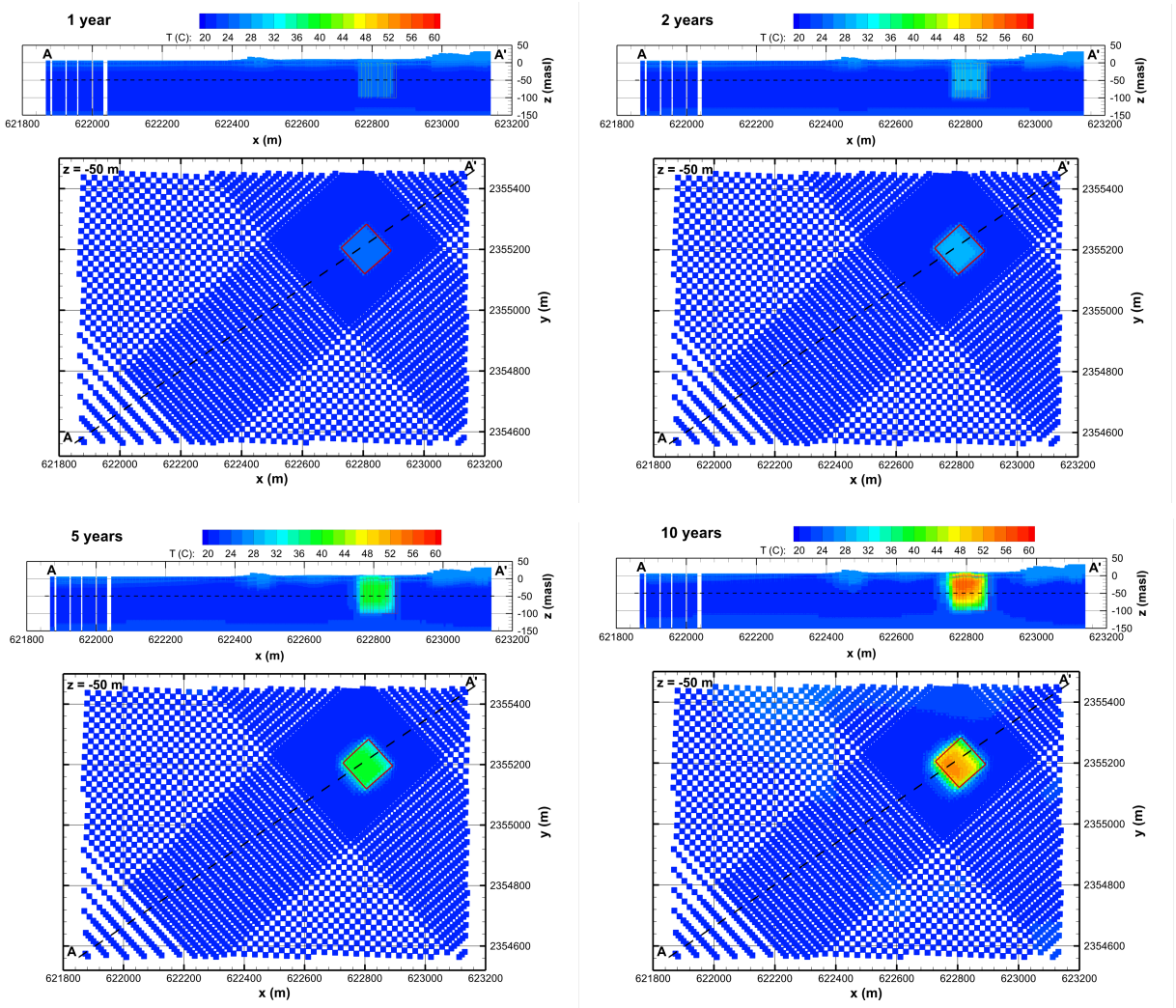

Figure B- 3. Effect of realistic initial temperature profile on TOUGH model results, for Case *D* with minimal groundwater flow